

University of Windsor

Scholarship at UWindor

Electronic Theses and Dissertations

Theses, Dissertations, and Major Papers

2007

Experimental study on the performance of a 10-cell proton exchange membrane (PEM) fuel cell stack

Jixin Chen
University of Windsor

Follow this and additional works at: <https://scholar.uwindsor.ca/etd>

Recommended Citation

Chen, Jixin, "Experimental study on the performance of a 10-cell proton exchange membrane (PEM) fuel cell stack" (2007). *Electronic Theses and Dissertations*. 4652.
<https://scholar.uwindsor.ca/etd/4652>

This online database contains the full-text of PhD dissertations and Masters' theses of University of Windsor students from 1954 forward. These documents are made available for personal study and research purposes only, in accordance with the Canadian Copyright Act and the Creative Commons license—CC BY-NC-ND (Attribution, Non-Commercial, No Derivative Works). Under this license, works must always be attributed to the copyright holder (original author), cannot be used for any commercial purposes, and may not be altered. Any other use would require the permission of the copyright holder. Students may inquire about withdrawing their dissertation and/or thesis from this database. For additional inquiries, please contact the repository administrator via email (scholarship@uwindsor.ca) or by telephone at 519-253-3000ext. 3208.

Experimental Study on the Performance of a 10-cell Proton Exchange Membrane (PEM)
Fuel Cell Stack

by

Jixin Chen

A Thesis
Submitted to the Faculty of Graduate Studies
through Mechanical Engineering
in Partial Fulfillment of the Requirements for
the Degree of Master of Applied Science at the
University of Windsor

Windsor, Ontario, Canada

2007

© 2007 Jixin Chen



Library and
Archives Canada

Bibliothèque et
Archives Canada

Published Heritage
Branch

Direction du
Patrimoine de l'édition

395 Wellington Street
Ottawa ON K1A 0N4
Canada

395, rue Wellington
Ottawa ON K1A 0N4
Canada

Your file *Votre référence*
ISBN: 978-0-494-34934-2
Our file *Notre référence*
ISBN: 978-0-494-34934-2

NOTICE:

The author has granted a non-exclusive license allowing Library and Archives Canada to reproduce, publish, archive, preserve, conserve, communicate to the public by telecommunication or on the Internet, loan, distribute and sell theses worldwide, for commercial or non-commercial purposes, in microform, paper, electronic and/or any other formats.

The author retains copyright ownership and moral rights in this thesis. Neither the thesis nor substantial extracts from it may be printed or otherwise reproduced without the author's permission.

AVIS:

L'auteur a accordé une licence non exclusive permettant à la Bibliothèque et Archives Canada de reproduire, publier, archiver, sauvegarder, conserver, transmettre au public par télécommunication ou par l'Internet, prêter, distribuer et vendre des thèses partout dans le monde, à des fins commerciales ou autres, sur support microforme, papier, électronique et/ou autres formats.

L'auteur conserve la propriété du droit d'auteur et des droits moraux qui protègent cette thèse. Ni la thèse ni des extraits substantiels de celle-ci ne doivent être imprimés ou autrement reproduits sans son autorisation.

In compliance with the Canadian Privacy Act some supporting forms may have been removed from this thesis.

Conformément à la loi canadienne sur la protection de la vie privée, quelques formulaires secondaires ont été enlevés de cette thèse.

While these forms may be included in the document page count, their removal does not represent any loss of content from the thesis.

Bien que ces formulaires aient inclus dans la pagination, il n'y aura aucun contenu manquant.


Canada

ABSTRACT

In this study, the steady state performance and dynamic behavior of a commercial 10-cell PEM fuel cell stack was experimentally investigated using a self-designed and developed PEM Fuel Cell Testing Stand. The start-up characteristics of the stack to different current load and dynamic responses after current step-up were studied. The stack voltage was observed to experience oscillation at air excess coefficient of 2 owing to the flooding and recovery of part of cells. To correlate the stack voltage with the pressure drop across the cathode/anode, fast Fourier transform was performed to obtain the dominant frequency of pressure drop signal, which indicated the water behavior in cathode/anode thereby predicting the stack voltage change. It is potentially possible to utilize pressure drop signal as a diagnosis tool for stack voltage at a fixed current load.

DEDICATION

To my Parents and my Teachers

ACKNOWLEDGEMENTS

From the bottom of heart, I would like to appreciate my advisor, Dr. Biao Zhou, for his guidance and supports during past two years. The knowledge, expertise and most importantly, attitude and characteristic I learnt from him will doubtless shape my future and direct me to success. He will be my forever advisor.

I would like to extend my acknowledgment to Dr. David Ting, Dr. Huapeng Wu and Dr. Gary Rankin for their time and assistance during the development of this thesis.

Technical supports from Mr. Andrew Jenner and Mr. Matthew St. Louis are greatly appreciated. Without their help I could not finish my project so smoothly and nicely. The friendship between us was also unforgettable.

Special thanks go to Mr. Kui Jiao, who is the closest group colleague and gave me countless help in past two years. Special thanks also go to Mr. Yawei Li, who is one of my best friends in Windsor. The numerous unsleeping nights of studying could become much more tedious and tiresome without the talking and refreshment breaks with him.

Furthermore, thanking my parents for their supports and love. They are the source of my courage and persistence.

Finally, financial supports from Auto21TM and NSERC are greatly acknowledged. The project could never proceed without the research grant.

TABLE OF CONTENTS

ABSTRACT	iii
DEDICATION	iv
ACKNOWLEDGEMENTS	v
LIST OF TABLES	vii
LIST OF FIGURES	viii
CHAPTER	
I. INTRODUCTION	
1.1 Fuel cell technology.....	1
1.2 Proton Exchange Membrane (PEM) fuel cell.....	1
1.3 PEM fuel cell system and performance	2
1.4 Research summary.....	3
II. REVIEW OF LITERATURE	
2.1 PEM Fuel cell performance	5
2.2 Fuel cell test system.....	14
2.3 Modeling and experimental studies	17
III. EXPERIMENTAL	
3.1 Experimental setup	21
3.2 Details of experiments	23
IV. RESULTS AND DISCUSSIONS	
4.1 Steady state cases.....	28
4.2 Start-up cases	31
4.3 Current step-up cases.....	63
V. CONCLUSIONS AND RECOMMENDATIONS	
5.1 Conclusions.....	81
5.2 Recommendations.....	82
REFERENCES	83
VITA AUCTORIS	85

LIST OF TABLES

TABLE 1. MASS FLOW RATES (SLPM) AT DIFFERENT CURRENT LOADS AND EXCESS COEFFICIENTS.....	25
TABLE 2 EXCESS COEFFICIENTS FOR DIFFERENT CURRENT STEP-UP CASES.....	27
TABLE 3. CHANNEL SPECIFICATIONS AND TIME TO PASS CHANNEL AT DIFFERENT CURRENT LOADS.....	48

LIST OF FIGURES

FIG. 1. SCHEMATIC OF PEM FUEL CELL OPERATION.....	5
FIG. 2. PEM FUEL CELL STRUCTURE [28].....	7
FIG. 3. TYPICAL STEADY-STATE PERFORMANCE CURVE OF PEM FUEL CELL [2].....	8
FIG. 4. SCHEMATIC OF CURRENT INTERRUPT TECHNIQUE [2].....	12
FIG. 5. SCHEMATIC OF TYPICAL FUEL CELL TEST SYSTEM [3].....	15
FIG. 6. SCHEMATIC OF THE PEM FUEL CELL TESTING STAND.....	22
FIG. 7. STACK POLARIZATION CURVE UNDER DIFFERENT AIR FLOW RATES.....	28
FIG. 8. STACK POLARIZATION CURVE UNDER DIFFERENT HYDROGEN FLOW RATES.....	29
FIG. 9. STACK POWER OUTPUT VERSUS CURRENT DENSITY UNDER DIFFERENT AIR FLOW RATES.....	30
FIG. 10. STACK POWER OUTPUT VERSUS CURRENT DENSITY UNDER DIFFERENT HYDROGEN FLOW RATES.....	31
FIG. 11. STACK VOLTAGE RESPONSE WHEN STACK STARTED FROM IDLE TO 1 A LOAD.....	32
FIG. 12. STACK VOLTAGE RESPONSE WHEN STACK STARTED FROM IDLE TO 2 A LOAD.....	33
FIG. 13. STACK VOLTAGE RESPONSE WHEN STACK STARTED FROM IDLE TO 4 A LOAD.....	34
FIG. 14. STACK VOLTAGE RESPONSE WHEN STACK STARTED FROM IDLE TO 6 A LOAD.....	35
FIG. 15. CHANGE OF TEMPERATURE WITH TIME WHEN STACK STARTED FROM IDLE TO 1 A LOAD.....	36
FIG. 16. CHANGE OF TEMPERATURE WITH TIME WHEN STACK STARTED FROM IDLE TO 2 A LOAD.....	37
FIG. 17. CHANGE OF TEMPERATURE WITH TIME WHEN STACK STARTED FROM IDLE TO 4 A LOAD.....	38

FIG. 18. CHANGE OF TEMPERATURE WITH TIME WHEN STACK STARTED FROM IDLE TO 6 A	
LOAD.....	38
FIG. 19. CHANGE OF PRESSURE DROP WITH TIME WHEN STACK STARTED FROM IDLE TO 1 A	
LOAD.....	40
FIG. 20. CHANGE OF PRESSURE DROP WITH TIME WHEN STACK STARTED FROM IDLE TO 2 A	
LOAD.....	42
FIG. 21. CHANGE OF PRESSURE DROP WITH TIME WHEN STACK STARTED FROM IDLE TO 4 A	
LOAD.....	42
FIG. 22. CHANGE OF PRESSURE DROP WITH TIME WHEN STACK STARTED FROM IDLE TO 6 A	
LOAD.....	43
FIG. 23. DOMINANT FREQUENCY VERSUS TIME PLOTS UNDER DIFFERENT WINDOW SIZES ..	51
FIG. 24. CHANGES OF DOMINANT FREQUENCY OF AIR/CATHODE PRESSURE DROP AND STACK	
VOLTAGE WITH TIME WHEN STACK STARTED FROM IDLE TO 1 A LOAD.....	53
FIG. 25. CHANGES OF DOMINANT FREQUENCY OF AIR/CATHODE PRESSURE DROP AND STACK	
VOLTAGE WITH TIME WHEN STACK STARTED FROM IDLE TO 2 A LOAD.....	55
FIG. 26. CHANGES OF DOMINANT FREQUENCY OF AIR/CATHODE PRESSURE DROP AND STACK	
VOLTAGE WITH TIME WHEN STACK STARTED FROM IDLE TO 4 A LOAD.....	57
FIG. 27. CHANGES OF DOMINANT FREQUENCY OF AIR/CATHODE PRESSURE DROP AND STACK	
VOLTAGE WITH TIME WHEN STACK STARTED FROM IDLE TO 6 A LOAD.....	58
FIG. 28. CHANGES OF DOMINANT FREQUENCY OF HYDROGEN/ANODE PRESSURE DROP AND	
STACK VOLTAGE WITH TIME WHEN STACK STARTED FROM IDLE TO 1 A LOAD	59
FIG. 29. CHANGES OF DOMINANT FREQUENCY OF HYDROGEN/ANODE PRESSURE DROP AND	
STACK VOLTAGE WITH TIME WHEN STACK STARTED FROM IDLE TO 2 A LOAD	60

FIG. 30. CHANGES OF DOMINANT FREQUENCY OF HYDROGEN/ANODE PRESSURE DROP AND STACK VOLTAGE WITH TIME WHEN STACK STARTED FROM IDLE TO 4 A LOAD	61
FIG. 31. CHANGES OF DOMINANT FREQUENCY OF HYDROGEN/ANODE PRESSURE DROP AND STACK VOLTAGE WITH TIME WHEN STACK STARTED FROM IDLE TO 6 A LOAD	62
FIG. 32. STACK VOLTAGE RESPONSES AFTER CURRENT STEP-UP WITH EXCESS COEFFICIENT FIXED AT 1.5 FOR AIR AND 1.2 FOR HYDROGEN	64
FIG. 33. STACK VOLTAGE RESPONSES AFTER CURRENT STEP-UP WITH EXCESS COEFFICIENT FIXED AT 3 FOR AIR AND 1.2 FOR HYDROGEN	65
FIG. 34. STACK VOLTAGE RESPONSE AFTER CURRENT STEP-UP FROM 1 A TO 2 A WITH EXCESS COEFFICIENT FIXED AT 2 FOR AIR AND 1.2 FOR HYDROGEN.....	66
FIG. 35. STACK VOLTAGE RESPONSE AFTER CURRENT STEP-UP FROM 1 A TO 3 A WITH EXCESS COEFFICIENT FIXED AT 2 FOR AIR AND 1.2 FOR HYDROGEN.....	67
FIG. 36. STACK VOLTAGE RESPONSE AFTER CURRENT STEP-UP FROM 1 A TO 4 A WITH EXCESS COEFFICIENT FIXED AT 2 FOR AIR AND 1.2 FOR HYDROGEN.....	68
FIG. 37. STACK VOLTAGE RESPONSE AFTER CURRENT STEP-UP FROM 1 A TO 6 A WITH EXCESS COEFFICIENT FIXED AT 2 FOR AIR AND 1.2 FOR HYDROGEN.....	69
FIG. 38. PRESSURE DROP RESPONSE AFTER CURRENT STEP-UP FROM 1 A TO 2 A.....	70
FIG. 39. PRESSURE DROP RESPONSE AFTER CURRENT STEP-UP FROM 1 A TO 3 A.....	71
FIG. 40. PRESSURE DROP RESPONSE AFTER CURRENT STEP-UP FROM 1 A TO 4 A.....	71
FIG. 41. PRESSURE DROP RESPONSE AFTER CURRENT STEP-UP FROM 1 A TO 6 A.....	72
FIG. 42. CHANGES OF DOMINANT FREQUENCY OF AIR/CATHODE PRESSURE DROP AND STACK VOLTAGE WITH TIME AFTER CURRENT DRAWN FROM STACK STEPPED UP FROM 1 A TO 2 A.....	73

FIG. 43. CHANGES OF DOMINANT FREQUENCY OF AIR/CATHODE PRESSURE DROP AND STACK VOLTAGE WITH TIME AFTER CURRENT DRAWN FROM STACK STEPPED UP FROM 1 A TO 3 A.....	74
FIG. 44. CHANGES OF DOMINANT FREQUENCY OF AIR/CATHODE PRESSURE DROP AND STACK VOLTAGE WITH TIME AFTER CURRENT DRAWN FROM STACK STEPPED UP FROM 1 A TO 4 A.....	75
FIG. 45. CHANGES OF DOMINANT FREQUENCY OF AIR/CATHODE PRESSURE DROP AND STACK VOLTAGE WITH TIME AFTER CURRENT DRAWN FROM STACK STEPPED UP FROM 1 A TO 6 A.....	76
FIG. 46. CHANGES OF DOMINANT FREQUENCY OF HYDROGEN/ANODE PRESSURE DROP AND STACK VOLTAGE WITH TIME AFTER CURRENT DRAWN FROM STACK STEPPED UP FROM 1 A TO 2 A	77
FIG. 47. CHANGES OF DOMINANT FREQUENCY OF HYDROGEN/ANODE PRESSURE DROP AND STACK VOLTAGE WITH TIME AFTER CURRENT DRAWN FROM STACK STEPPED UP FROM 1 A TO 3 A	78
FIG. 48. CHANGES OF DOMINANT FREQUENCY OF HYDROGEN/ANODE PRESSURE DROP AND STACK VOLTAGE WITH TIME AFTER CURRENT DRAWN FROM STACK STEPPED UP FROM 1 A TO 4 A	79
FIG. 49. CHANGES OF DOMINANT FREQUENCY OF HYDROGEN/ANODE PRESSURE DROP AND STACK VOLTAGE WITH TIME AFTER CURRENT DRAWN FROM STACK STEPPED UP FROM 1 A TO 6 A	80

CHAPTER I

INTRODUCTION

1.1 Fuel cell technology

A fuel cell is a device that generates electricity by a chemical reaction. Fuel cells have been proposed as an ideal power source for a variety of applications such as automotives and substitute batteries due to their significant advantages, i.e. high efficiency, low emission, silence and simplicity [1]. It is widely accepted that fuel cells will finally replace the traditional internal combustion engines to be used in vehicular applications. Over past decades fuel cell technology has achieved numerous improvements in terms of output performance, durability, stability, cost and system integration. However, it is still far beyond a mature technology mainly because 1) fuel cell itself must achieve higher efficiency and lower cost before successful commercialization; 2) fuel cell power system is complicated system and essentially new technology under active research.

1.2 Proton Exchange Membrane (PEM) fuel cell

Nowadays PEM fuel cell is the most popular one under research and development compared with other mainstream types of fuel cell, i.e., direct methanol fuel cell (DMFC), alkaline fuel cell (AFC), phosphoric acid fuel cell (PAFC), molten carbonate fuel cell (MCFC) and solid oxide fuel cell (SOFC). This is mainly because the high power density and low operating temperature make the PEM fuel cell uniquely suitable for portable power and automotive applications. PEM fuel cell appears to offer the best prospect for

further improvement until the successful commercialization, which may become true within two decades.

1.3 PEM fuel cell system and performance

Due to the complex electrochemistry, PEM fuel cell itself is an unsteady system, which is very sensitive to several operating parameters such as the reactant gas supply rate and humidity, system pressure and stack temperature. The output of fuel cell may vary significantly even one of those parameters changes. Therefore a well-developed control system is indispensable for PEM fuel cell operation to maintain significant parameters in a steady state and to adjust necessary parameters upon the user's requirement. A stand-alone PEM fuel cell stack can never be utilized as the power supply and only when the control system is integrated can it be termed as a complete "fuel cell system" or power supply module. Development of control system for PEM fuel cell is a paramount step for any power supply application.

On the other hand, the dynamic behavior of PEM fuel cell has not been fully studied and understood. The experimental studies on the dynamic behavior is few in literature, probably because the requirement on testing instrument and technique and the unawareness of its importance before. Additionally, due to the complexity and unsteadiness during the electrochemical reaction, reactant mass transport as well as water and thermal management, the transience of PEM fuel cell after start-up/load change is more difficult to model than the steady-state performance. Some important modeling approaches to study the dynamic behavior have been reported in literature in recent years;

however the corresponding experimental data lack to provide verification for those modeling results. It has been gradually realized that studies on the dynamic behavior is extremely important as the fuel cell stack will always experience transience during start-up, shut-down and switch of power requirement in portable and automotive applications. The identification of physics behind the dynamic behavior and the proposal of corresponding control method during transience will provide solution for improving stack durability, efficiency and optimizing system development. It should be noted that in terms of fuel cell itself, other issues such as optimum design of membrane electrode assembly (MEA) and flow channel may be of most importance; whereas from the view of a power system, those two points mentioned above are more urgent and significant in PEM fuel cell research.

1.4 Research summary

This study will therefore focus on these two points: system development and experimental study on the performance of a commercial fuel cell stack, especially the dynamic behavior. A PEM fuel cell testing stand was self-designed, built and configured. The testing stand is able to monitor and/or control all necessary operating parameters including reactant gas flow rate and humidity, system pressure, pressure drop across the anode/cathode, stack and gas temperature, cell voltage, current and power output. The testing stand also features a friendly user interface developed in LabVIEW environment, where codes implement measurement data acquisition and display and real-time control of hardware. With the aid of the testing stand, the steady state and dynamic performance of a commercial 10-cell PEM fuel cell stack ordered from Palcan Power Systems Inc.,

Vancouver was experimentally investigated. The cathode/anode pressure drop and stack voltage during transience was correlated, both being analyzed from the view of water behavior in the cell. In the meantime, the functionality and performance of the self-developed testing stand was verified.

CHAPTER II

REVIEW OF LITERATURE

2.1 PEM Fuel cell performance

2.1.1 PEM fuel cell fundamentals

PEM fuel cell is an electrochemical energy conversion device that produces electricity from external supplies of fuel (on the anode side) and oxidant (on the cathode side). Reactions at both sides are as follows:

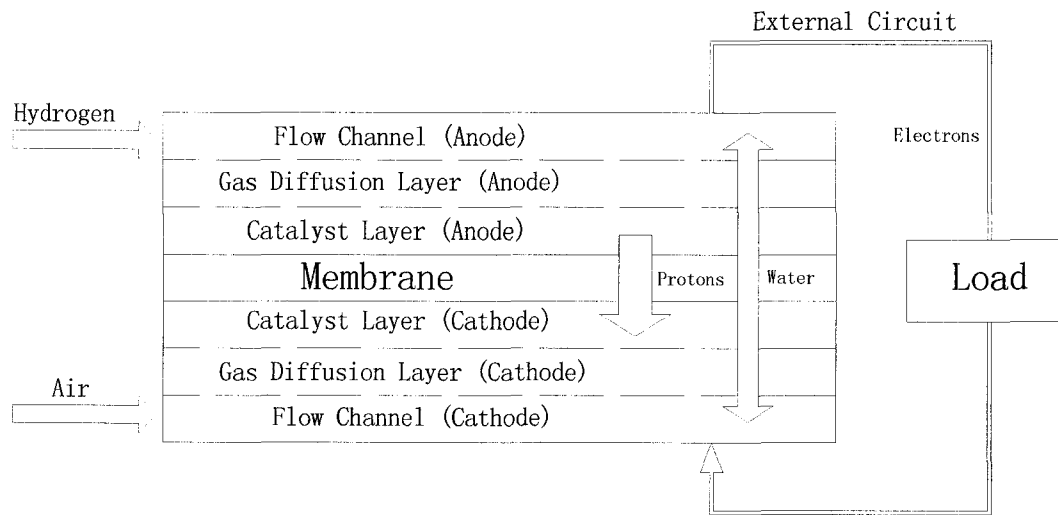
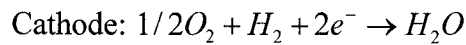
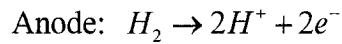


Fig. 1. Schematic of PEM fuel cell operation

Hydrogen ions released at the anode pass through the Nafion (®Dupont) membrane, the industrial standard for PEM fuel cell, to reach the cathode and participate the oxidization reaction. In the meantime, the membrane blocks the electrons to pass

through so that they can only transport via the external circuit to reach the cathode. The movement of bulk electrons, as known to all, is the way how current generates.

At both sides of the membrane, the electrode forms in terms of carbon supported platinum as the catalyst. PEM fuel cell usually works at 60-80 C and normal pressure, which means presence of catalyst is significant to facilitate the electrochemical reaction. Platinum is the best catalyst for both anode and cathode, although some substitutes such as Pt alloyed compound are currently under active research. The very thin (typically 0.03 mm) layer of carbon supported platinum is named catalyst layer.

As the physical support of the membrane and catalyst layer, gas diffusion layer is attached to the outside of the catalyst layer and the whole structure (membrane, catalyst layer and gas diffusion layer) is compressed to form the Membrane Electrode Assembly (MEA). Carbon paper or carbon cloth is widely used as the gas diffusion layer because of its high porosity that facilitates the reactant transportation towards the catalyst sites. Also the very low electrical resistance of carbon paper/cloth makes the ohmic loss within an acceptable range.

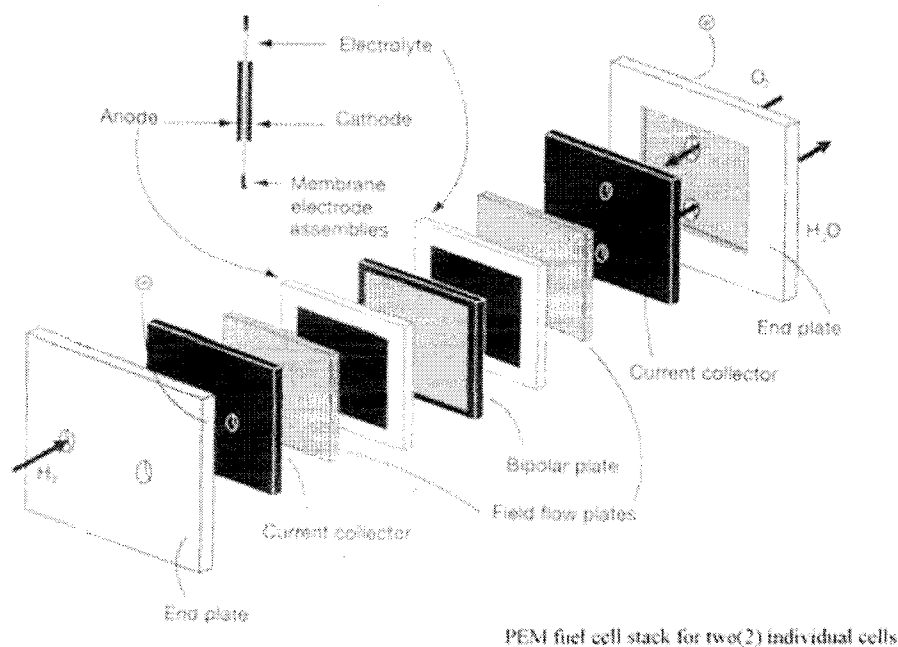


Fig. 2. PEM fuel cell structure [28]

The open circuit voltage (OCV) of a single cell is very small with a theoretical value of 1.18 V, given the product of water is liquid and at a temperature of 80 [1]. It should be noted that this figure is the reversible open circuit voltage that does not take into account any loss or irreversibility. The operating voltage is even smaller, about 0.7 V when drawing a useful current. Consequently, many cells have to be connected in series to produce a useful voltage. To this end, “bipolar plate” is made, as it is the interconnection between the anode of one cell and the cathode of the neighboring cell. There are channels cut in both sides of the bipolar plate so that the reactant gas can flow over the face of electrode. In the meantime, it makes a good electrical contact with the surface of electrode, which is achieved by 1) the material is very low-resistant; 2) the whole stack is compressed evenly during assembling. The material for bipolar plate is usually stainless steel or graphite.

2.1.2 Steady-state performance and irreversibility

The performance of a fuel cell is usually summarized with a graph of its current–voltage outputs. This graph, called a current–voltage (I–V) curve, shows the voltage output of the fuel cell at a given current output. The current has been normalized by the area of the fuel cell in terms of a standard unit of current density (in amperes per square centimeter). Larger fuel cells can obviously produce more electricity than smaller ones; therefore a normalized current unit makes fuel cell performance comparable.

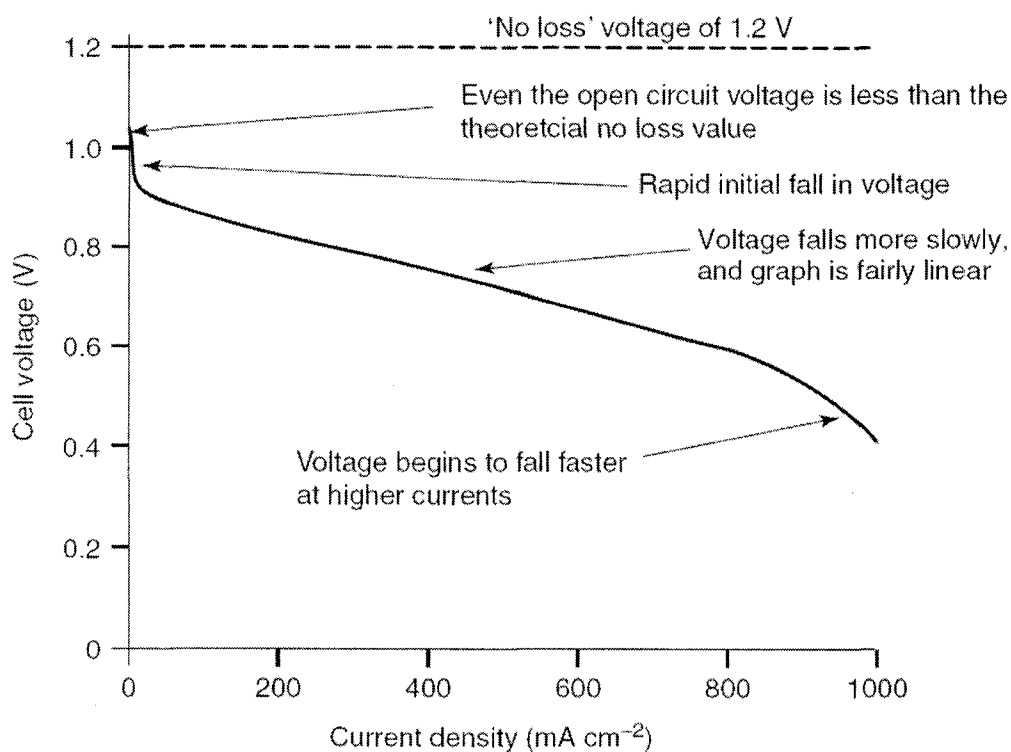


Fig. 3. Typical steady-state performance curve of PEM fuel cell [2]

Theoretically, a fuel cell would supply any amount of current under the condition of sufficient fuel supply, while maintaining a constant voltage determined by

thermodynamics. In practice, however, the actual voltage output of a fuel cell is less than the ideal thermodynamically predicted value. Furthermore, the more current that is drawn from a real fuel cell, the lower the voltage output of the cell, limiting the total power that can be delivered.

It is difficult to maintain the cell voltage at a high level under current load, as shown in the above figure. The voltage output of a fuel cell in operation is less than thermodynamically predicted value due to irreversible losses. Total loss increases with the increasing current drawn from the stack. There are three major types of fuel cell losses, which shape a fuel cell I–V curve.

1) Activation loss. Such loss is caused by the slowness of the reactions taking place on the surface of the electrodes. A proportion of the voltage generated is lost in driving the chemical reaction that transfers the electrons to or from the electrode. Electron does not participate the reaction as soon as it releases, enough amount of electrons accumulate to such a level that the reaction can take place continuously given the sufficient gas supplies. This level can be imagined, or is equivalent to, the activation loss. In the figure above, it is represented by the initial sharp drop of the cell voltage.

2) Ohmic loss. It is the straightforward resistance to the flow of electrons through the material of the electrodes and the various interconnections, as well as the resistance to the flow of ions through the electrolyte. This voltage drop is essentially proportional to

current density, represented by the linear fall in the middle of the performance curve in the figure.

3) Mass transport or concentration loss. Such loss results from the change in concentration of the reactants at the surface of the electrodes as they are consumed along the gas channel from the inlet to the outlet. Concentration affects voltage via the change of differential pressure of reactant. That is why this type of irreversibility is called concentration loss. On the other hand, since the reduction in concentration is the result of a failure to transport sufficient reactant to the electrode surface or catalyst sites, this type of irreversibility is also called mass transport loss. In the figure above, such loss can be observed at high current density range as an unlinear drop, because sufficient reactant supply is the controlling factor to obtain large amount of current.

4) Fuel crossover and internal currents. Such loss results from the waste of fuel passing through the electrolyte, and, to a lesser extent, from electron conduction through the electrolyte. The electrolyte should only transport ions through the cell, however very small amount of fuel diffusion and electron flow will always be possible. It does have a marked influence on the OCV of low-temperature fuel cell, which explains why the OCV is always smaller than the theoretical no loss value.

Combining all the irreversibilities, the operating voltage of a fuel cell at a current density i can be modeled by the following equation [2]:

$$V = E - \Delta V_{ohm} - \Delta V_{act} - \Delta V_{trans} = E - ir - A \ln\left(\frac{i + i_n}{i_0}\right) + m \exp(ni)$$

Where i_n is the internal and fuel crossover equivalent current density; A the slope of the Tafel line; i_0 exchange current density; m and n the constants in the mass transport overvoltage; r the area specific resistance.

2.1.3 Dynamic performance

It should be noted the I-V curve describes the steady-state performance of the fuel cell. “Steady state” means the performance is time-independent or time-invariable. To obtain the curve, either the current or the voltage is set as a constant, the corresponding voltage or current is determined by the electrochemistry of the fuel cell system. Enough pairs of I-V data can then produce the performance plot.

However, steady-state performance is far from providing enough information of a fuel cell system. The reason for researchers and engineers to obtain the fuel cell performance is to know physics of fuel cell operation, to distinguish good design from bad one and to find the source for performance decay. To this end, much more information is necessary such as discrimination among different losses from a total loss measured as the voltage drop. More advanced characterization tools and techniques are applied to acquire the dynamic performance, as a comparison to the steady-state.

It is straightforward that the dynamic performance is time-dependent, time is always one variable in the performance curve. One technique that is usually used in characterization is the current interrupt measurement. A current as a step change to the original current is abruptly drawn from the stack at time $t = 0$ and the system voltage

response approaching to steady state is measured. In practice, such step change usually means the sudden cut-off of current, which can be performed simply by a switch and an oscilloscope as shown in the figure below.

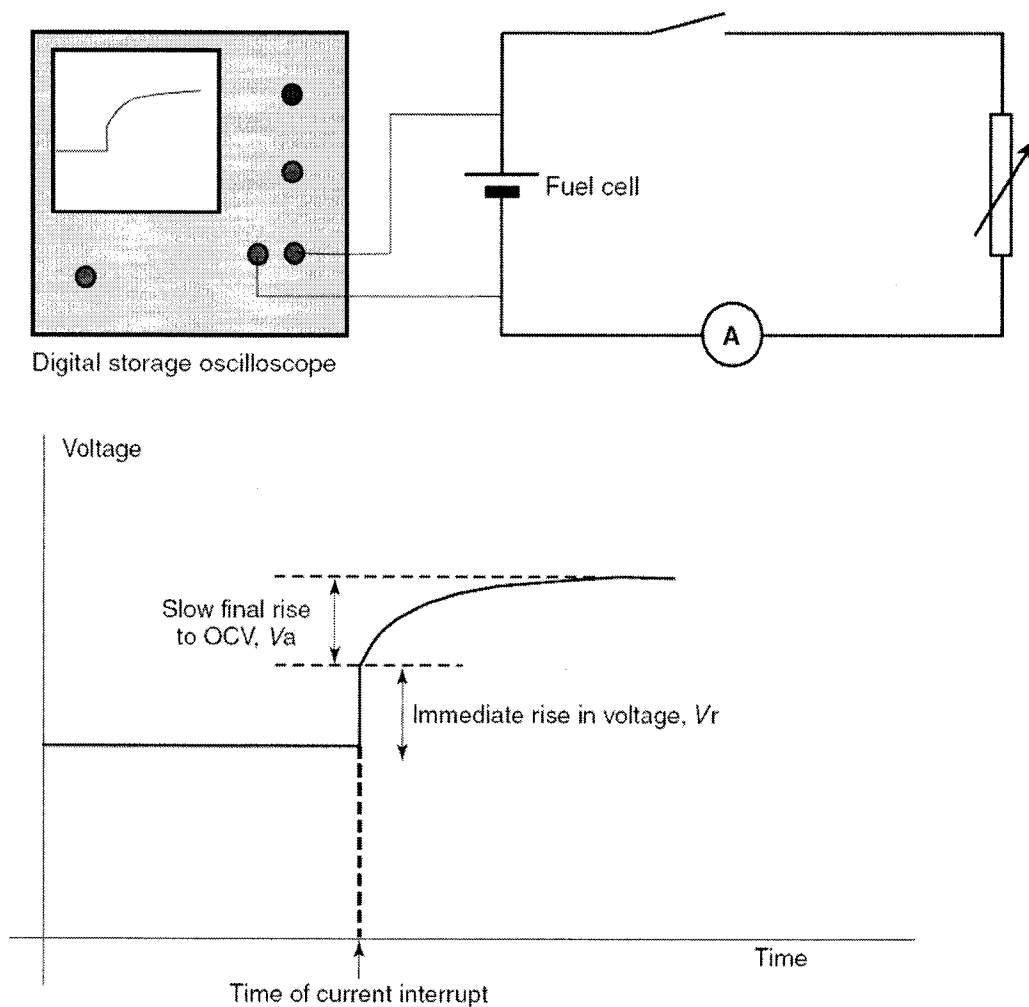


Fig. 4. Schematic of current interrupt technique [2]

From the voltage response, ohmic loss and activation loss can be distinguished. The former reduces to zero immediately whereas the latter take some time to release due to the charge double layer effect. Accordingly, in the figure above the immediate voltage

rise represents ohmic loss and the subsequent slow rise to the final state represents activation loss.

In recent years some fuel cell research group also tried observing the current transient response with a step change in cell voltage. The current overshoot/undershoot was observed [13] [14], which is sensitive to the operating conditions. These information help researchers understand the electrochemical physics of fuel cell operation and furthermore, provide useful data for fuel cell application development such as power for automotive. During the load changes, current surges are always detrimental to most onboard devices. Therefore the dynamic performance should have been well examined in laboratory and special technique should be developed to prevent surges. Fuel cell companies always focus more on the dynamic performance as in the real case what is concerned by the user is the voltage/current output over time, not the steady-state performance that may need a long time to reach. Steady-state performance resembles the nominal or rated output, however rarely the real performance that is obtained by user.

Another technique as a useful research tool is the Electrochemical Impedance Spectroscopy (EIS). In this dynamic technique, a sinusoidal perturbation (usually a voltage perturbation) is applied to a fuel cell system and the amplitude and phase shift of the resulting current response are measured. Measurements can be conducted over a wide range of frequencies, resulting in the construction of an impedance spectrum. This technique requires special instrument such as an impedance analyzer to generate high-frequency signal. Impedance plot over a wide range of frequencies (usually from 0 to

100,000 Hz) can distinguish different losses in a more detailed fashion than current interrupt method. The disadvantage is that it is an expensive and time-consuming characterization tool.

In summary, both steady-state and dynamic performance are important data, providing useful information to researchers and designers. The former focuses on the stabilized output given a specific operating condition whereas the latter presents the instability in output over a period of time. In experimental studies, usually both performances are investigated to present complete information of the fuel cell.

2.2 Fuel cell test system

Figure below presents a diagram of a basic test station used for in situ fuel cell characterization. This diagram is specifically for a PEM fuel cell; however a similar setup could be implemented for any other type of fuel cell. Since fuel cell performance strongly depends on the operating conditions, a good test setup allows flexible monitor and control over operating parameters such as but not limited to pressure, temperature, relative humidity, and flow rate of the reactant gases. The first and foremost purpose of the fuel cell test system is to establish a stabilized and controllable operating condition, under which the fuel cell performance can be measured. Also the system should be friendly interfaced with the end user and be stable, accurate and safe.

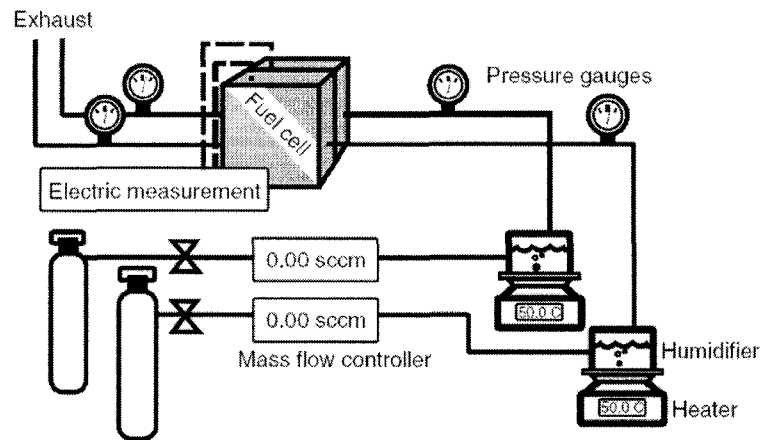


Fig. 5. Schematic of typical fuel cell test system [3]

In the market various commercial PEM fuel cell test systems are available. For fuel cell research groups, it is obviously a good practice to purchase a commercial test station to conduct experimental studies. Because it is time-saving, and the functionality and safety of the instrument are always guaranteed by the company. In literature many groups mentioned the commercial test system that is used in the experiments. Liu et al. [4] studied the durability of PEM fuel cell MEA under dynamic testing conditions using a test station from Fuel Cell Technologies Inc. Hogarth et al. [5] investigated the performance of a self-humidifying PEM fuel cell with the aid of a Globetech test station (Globetech Inc., GT-1000), which is specifically suitable for single cell testing. Park et al. [6] studied the cross flow through the gas diffusion layer in the neighboring serpentine gas channels both experimentally and numerically. An automated fuel cell test station (Hydrogenics Inc., FCATS S-800) was used in their experiments.

Several companies are specifically developing fuel cell research related equipment. TesSol Inc. at Taxes offers fuel cell test stations for not only PEM but other

type fuel cells as well as catalyst test systems [7]. Fideris test station from TesSol features their patented technology in gas humidification management. Electrochem Inc. is another main company offering various fuel cell test station and other related equipment with a wide selectable range for different configurations [8]. All the companies mentioned here occupy the mainstream market and almost all test systems for fuel cell research are purchased from them.

Usually such a commercial test station consists of reactant supply module, humidification module, operating parameter control/monitor module, fuel cell performance control/monitor module, hydrogen safety module and data acquisition and communication module. The commercial test system always presents the advantage of good stability and safety. However the main disadvantage is that it is black-box fashion without flexibility in function change and it is usually very expensive. Such a test station mentioned above usually costs more than \$22,000 for a basic module, which is not cost-effective as a great portion of cost is for the unnecessary features such as large stainless steel housing. Unless a customized order, it is almost impossible to find every function necessary and every measurement range well suitable. For example, the test equipment from Electrochem Inc. mentions the gas pressure measurement range of 60 psig in maximum, which is beyond the system pressure limit of most small stacks. It is very rare to run small stack at system pressure higher than 3 atm, even in experiments. Therefore, the regulator included in the system may cost more than what is actually needed. From the author's view, purchase of a commercial system is not the best solution. Instead, the testing system was self-developed in this project.

2.3 Modeling and experimental studies

Many mathematical modeling studies on PEM fuel cells can be found in literature. One of the most widely cited steady state models is developed by Dutta et al. [9], however their model ignores the MEA thickness and membrane water storage and cannot be applied in transient analysis. In this paper, the author focuses on review of the dynamic fuel cell modeling studies. One of the earliest dynamic models was developed by Amphlett et al. [10], which predicted the cell voltage, power and stack temperature as a function of time when stack experienced perturbation. This model considers the stack as a whole (without consideration of temperature gradient and local current variation) to develop the model as it is the earliest attempt in modeling study. Ceraolo et al. [11] developed a simplified (one dimensional and single phase) dynamic model for PEM fuel cell and implemented the model in the Simulink environment. Although their model has neglected several important factors, they presented a detailed and new approach to determine the numerical values of the model parameters. Berning et al. [12] reported a three dimensional and multiphase model, which considered the gas transport and heat transfer process within the gas diffusion layer, flow channels and coolant channels. Xue et al. [13] developed a system-level dynamic model for PEM fuel cell that incorporates the complicated temperature, gas flow through the channel and the double charged layer effect in MEA under operating conditions. Their model features the application of three separate control volume. Recently Shimpalee et al. [14] [15] used the commercial computational fluid dynamics (CFD) solver to simulate the transient response of a PEM fuel cell subjected to a variable load and particularly focused on the overshoot/undershoot

behavior under different flow stoichiometry conditions. Their modeling study is based on their previous experimental observation of overshoot/undershoot in transience. Yu et al. [16] developed a water and thermal management model to study the steady-state and dynamic performance of Ballard PEM fuel cell stack, a famous commercial product in market. Their results showed the stack usually takes about 30-40 minutes to reach the steady state, which is further verified by the real operation. Wang et al. [17] [18] developed a three dimensional dynamic model considering all the important transient processes in PEM fuel cell including gas transport, water accumulation in membrane and double layer discharge. Their model is one of the most advanced models currently available in literature, which also predicts the overshoot/undershot during the step changes under some operating conditions.

Experimental studies on PEM fuel cell dynamic behavior are few in open literatures. Hamelin et al. [19] studied the transience of a PEM fuel cell under fast load communications and reported the faster fuel cell system response time than the load communications. The dynamic behavior of an air-breathing PEM fuel cell was experimentally investigated by Morner et al. [20], who focused on the transient effects of temperature, humidity and air flow rate. Kim et al. [21] [22] reported the influences of reservoirs, fuel dilution and gas stoichiometry on the dynamic behavior during load changes and they observed the overshoot/undershoot of the current density during cell voltage switch. This is an important phenomenon that indicates the physics of the dynamic behavior of PEM fuel cell; however it is still not well understood and controlled. Recently Yan et al. [23] conducted an investigation on the dynamic behavior of PEM fuel

cell under a series of changing parameters, i.e., the feed gas humidity, temperature, feed gas stoichiometry, air pressure, fuel cell size and flow channel pattern. The authors reported that all of those parameters have significant influence on the transient response. Although they provided an overall experimental data for validation of related fuel cell models, they did not focus on any parameter to further identify the effects on the transience. Philipps et al. [24] explored the behavior of a dynamically operated large-scale (11.5 kW) fuel cell system. Their research shows that a power-dependent modulation of the feed gas pressure and flow rate is necessary to achieve high energy efficiency.

It should be noted that although more and more experimental studies have been performed on dynamic behavior of PEM fuel cell and found in literature, the research is still at initial stage. Most publications display the bulk experimental data during the transience under various operating conditions; however the significant physics that result the unique transient response observed in the experiments, such as water flooding and removal, have not been thoroughly studied and understood. On the other hand, study on the dynamic behavior of a PEM fuel cell stack is very few in literature compared with single cell. Dynamic behavior of a single cell and a stack is completely different, which can be theoretically explained by the more complicated mass transport, local current distribution and water management. Such difference has also been experimentally observed [23]. For example, it is evident that for dynamic behavior of a fuel cell stack, one or several cells may experience serious output decay while others remain normal status in the meantime, which is detrimental to the stack durability. Therefore, it is

necessary and worthwhile to investigate the dynamic behavior of a stack so as to provide experimental data for stack design and system control. Finally, the unstable voltage has been observed as a significant phenomenon in dynamic behavior. However, few studies have focused to correlate such voltage change in transience with pressure drop across cathode/anode, which is potentially a diagnosis tool for controlling stack output. Barbir et al. [25] and He et al. [26] conducted some initial studies on pressure drop as a diagnosis tool for water flooding in PEM fuel cell, however they investigated steady cases only and did not explore the general relationship between pressure drop and cell voltage. Therefore, their methodology and conclusion may not be applicable for a different case; although as initial attempts their findings were of great significance. There is hardly any other publication in literature that concerns pressure drop as a diagnosis tool in fuel cell operation. A more systematic and detailed study on pressure drop as a diagnosis tool in dynamic stack operation is thus very necessary, which not only aids the understanding of physics in stack dynamic behavior but also extends the previous research with regard to pressure drop.

CHAPTER III

EXPERIMENTAL

In the study a 10-cell commercial PEM fuel cell stack from Palcan was operated under a variety of conditions using the self-developed PEM fuel cell testing stand. Information regarding the test system can be found in Section 3.1. The author would like to address that the overall performance of the Palcan stack under test is not satisfactory in terms of maximum current density it can reach, however the purpose of the study is to present the steady state and dynamic behavior and explore the physics behind; it is not aimed to show the superiority of the design of Palcan fuel cell stack.

3.1 Experimental setup

A PEM fuel cell testing stand was successfully developed as part of the project. It can monitor and/or control all operating parameters relating to PEM fuel cell performance including mass flow rate of the reactants, absolute pressure of the reactants and pressure drop across cathode/anode, stack temperature and gas temperature at inlet/outlet, humidity of the reactants before entering the stack, current drawn from stack, stack voltage and power. It features self-developed LabVIEW codes that is friendly interfaced with users, which can implement the instrument control, display and record data in a real-time format, and monitor the necessary parameter to prevent danger such as stack overheating. Not only the steady state performance, but also the dynamic behavior of PEM fuel cell can be studied with the aid of the test stand due to its programmable instrument control and data logging. Finally, the test stand is physically compact and low-cost compared with a commercial system that has similar functionality. A schematic

drawing of the self-developed system is shown in Fig. 6. Due to the limited space, detailed information of the system is not presented in this paper.

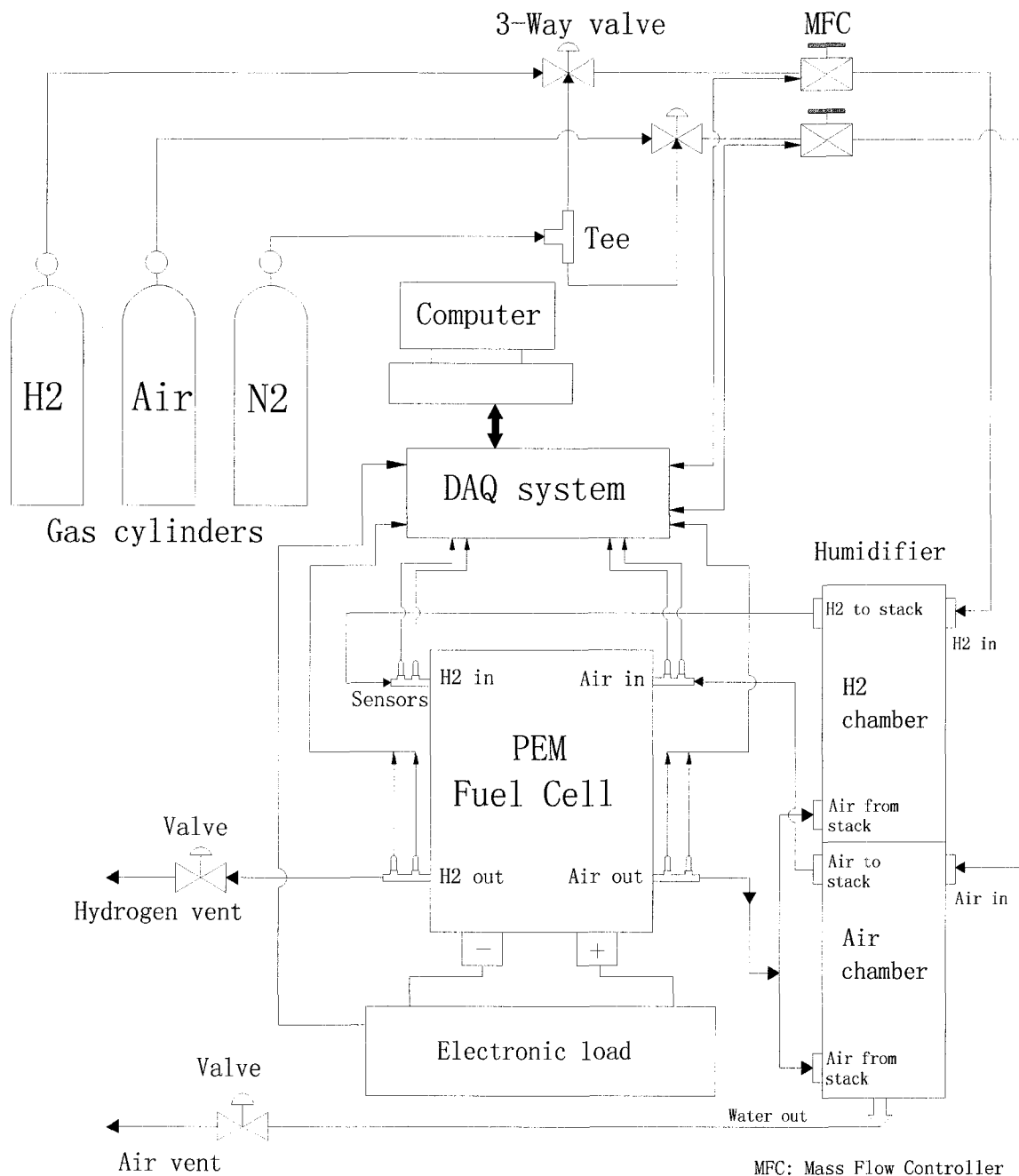


Fig. 6. Schematic of the PEM fuel cell testing stand

3.2 Details of experiments

Following experiments were conducted: 1) the steady state cases, i.e., the I-V curve acquisition under different Air/Hydrogen mass flow rates. This is to present the overall performance of the stack. 2) The start-up cases, i.e., the dynamic behaviors in terms of stack voltage, temperature, pressure drop when the stack starts from idle to different current loads were recorded and analyzed. The purpose is to find out the relationship between air/hydrogen pressure drop across the stack and the stack voltage, the former being potentially a diagnosis tool for the latter. The author believes such relationship exists and attempted to find it although no similar study has been found in literature. 3) The current step-up cases, i.e., the current drawn from the stack steps up from 1 A to different new levels and stack voltage and pressure drop transience were recorded and analyzed. Before step-up the stack performance is stable at 1 A. After step-up it may or may not reach a new steady state based on excess coefficient. Still it is attempted to reveal the relationship between air/hydrogen pressure drops and stack voltage.

3.2.1 Steady state cases

The electronic load was set to work as constant current mode so that the current drawn from the stack was fixed. To obtain the steady state I-V curve, increase the current from 0.5 A to maximum value it can draw, with a step variance of 0.5 A. At every current setpoint, wait for long enough time until the stack voltage is stable. This process may take several minutes or longer, also it is under some condition that a steady state cannot be achieved. Record the voltage value only when it is stable. To see the influence of mass flow rate on the I-V curve, there are two ways to set it at a given current setpoint. First, it

is determined by excess coefficient, i.e., mass flow rates of reactants increase with the current setpoint during experiments. The definition of excess coefficient λ at a given current load is as follows [27]:

$$\lambda = \frac{\text{Actually supplied mole number of air (oxygen) or hydrogen}}{\text{Theoretically consumed mole number of air (oxygen) or hydrogen}}$$

Every curve obtained via connecting I-V pairs in sequence is therefore characterized by “identical excess coefficient”. Second, set the mass flow rate at a constant value so that even at the maximum current load, it is sufficient in terms of theoretical calculation values. For example, it is set such that excess coefficient $\lambda = 2$ for air and 1.2 for hydrogen at the possible maximum current, which is estimated by experimental attempts. Obviously for a lower current setpoint, λ would be higher. Every curve obtained via connecting I-V pairs in sequence is therefore characterized by “identical mass flow rate”.

In the study the second approach was used since the stack voltage may experience oscillation during current step-up such as from 1 A to 1.5 A if λ maintains (applying first approach). Such oscillation may hardly stop, reason being discussed in next Chapter. That is to say, a steady state may never be reached if operating the stack in “constant λ mode” to obtain I-V curve. Refer to the table below, the air flow rates were selected as 1.47, 1.97, 2.48 and 2.95 SLPM respectively to obtain four I-V curves, hydrogen flow rate being 0.603 SLPM; the hydrogen flow rate were selected as 0.497, 0.623 and 0.828 SLPM respectively to obtain three I-V curves, air flow rate being 2.48 SLPM. The system pressure during operation was 1 local atmosphere (the same for all other cases below if not specified) since both anode and cathode were left open-ended. Mass flow rates and current drawn from stack were controlled, whereas stack voltage, temperature,

humidity were determined by the electrochemistry and system configuration. The current density was calculated at a given effective MEA area of 36 cm².

Current (A)	Air Excess Coefficient				Hydrogen Excess Coefficient			
	1	1.5	2	4	1	1.2	1.5	2
1	0.1658	0.2487	0.3316	0.6634	0.0696	0.0835	0.1044	0.1392
2	0.3317	0.4976	0.6634	1.3266	0.1393	0.1672	0.2090	0.2786
3	0.4975	0.7463	0.9950	1.9900	0.2089	0.2507	0.3134	0.4178
4	0.6633	0.9950	1.3266	2.6532	0.2786	0.3343	0.4179	0.5572
6	0.9950	1.4925	1.9900	3.9800	0.4179	0.5015	0.6269	0.8358
10	1.6583	2.4875	3.3166	6.6332	0.6965	0.8358	1.0448	1.3930

Table 1. Mass flow rates (SLPM) at different current loads and excess coefficients

3.2.2 Start-up cases

Start-up characteristic is an important measure of the PEM fuel cell dynamic behavior. As known to all, PEM fuel cell features cold start-up due to the relatively low operating temperature. However, such cold start-up may not readily achieve steady state at given excess coefficient and current load conditions. Stack voltage was observed to oscillate after start-up and such oscillation had no sign to stop even operating for several hours. This dynamic behavior of oscillation is the focus of the study.

The stack was started from idle to 1, 2, 4, 6 A constant current load respectively, with stack voltage and other operating parameters monitored and recorded. Based on the operating experience in steady cases, it was difficult to draw current higher than 6.5 A from the stack. Therefore current setpoints of 1, 2, 4, 6 A represent different load levels available for current stack. For every case, the mass flow rates of reactants were determined by excess coefficient, 2 for air and 1.2 for hydrogen. These excess coefficient values were selected such that the stack voltage oscillation would happen. As mentioned,

it is the focus of the study and the author would like to find out the physics behind. The mass flow rates were set when the load was disconnected, and remained unchanged during the whole experiment. When the reading from mass flow controller was stable, the load was connected to work at the constant current level. The moment when the load was connected was set as zero, therefore negative time ticks correspond to the small amount of data recorded before connecting the load. It should be noted that the electronic load took very short time (less than 1 second) to reach the current setpoint, thus it can be approximately considered all stack voltage response after zero time tick correspond to constant current load, or, the current setpoint.

Besides the stack voltage, changes of temperatures at stack surface, anode outlet and cathode outlet and reactant pressure drops across anode and cathode (air and hydrogen) were also plotted and analyzed.

3.2.3 Current step-up cases

Current step-up cases were performed in a similar fashion with the start-up cases. Instead of idle, the stack was first stabilized at 1 A current load, followed by increasing the current setpoint to 2, 3, 4, 6 A respectively. For both air and hydrogen, the excess coefficient remained unchanged before and after current step-up. Thus the mass flow rate setpoints were increased together with the current setpoint at the moment that was referenced as zero. However, due to the different settling time of mass flow controller and electronic load, the new current setpoint can be achieved before the mass flow rate setpoints with an advance of 2-3 seconds. Hence, right after the trigger of current/flow

rate step-up (time zero), the stack was working under insufficient reactant supplies for a very short time (less than 2 seconds). After that, mass flow rates reached the setpoints and excess coefficient can be therefore maintained.

Three cases were run in terms of different excess coefficients for air. Every case contains four sub-cases in terms of different current setpoint after step-up. It was found that hydrogen excess coefficient has very limited influence on the stack dynamic behavior as long as it is larger than 1.1. On the contrary, air excess coefficient has apparent and direct effects on the stack dynamic behavior, which was therefore varied to show behavior differences.

	Case 1 (Scarce)	Case 2 (Normal)	Case 3 (Excess)
Excess coefficient for air	1.5	2	3
Excess coefficient for hydrogen	1.2	1.2	1.2

Table 2 Excess coefficients for different current step-up cases

CHAPTER IV

RESULTS AND DISCUSSIONS

4.1 Steady state cases

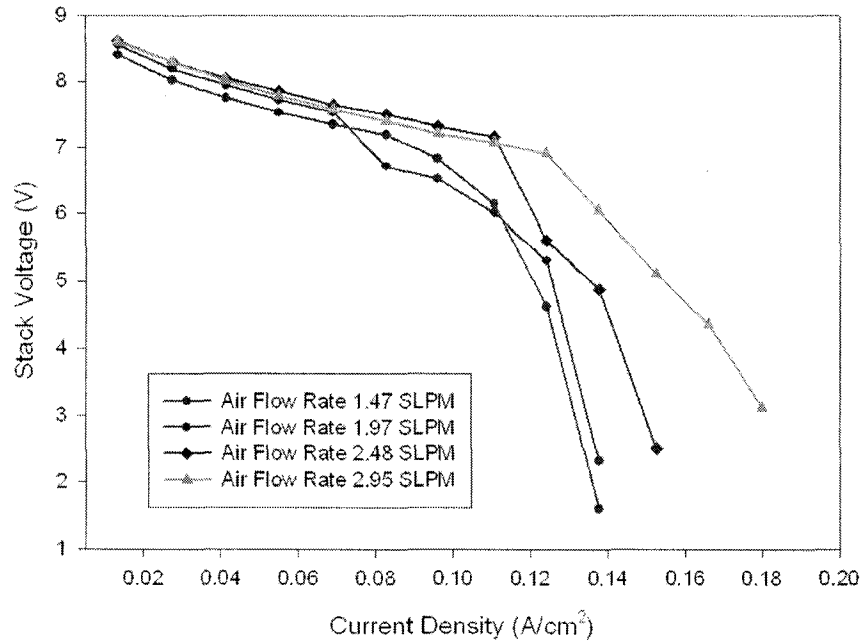


Fig. 7. Stack polarization curve under different air flow rates

As shown in Fig. 7, the overall steady state performance improves with the increase of air flow rate. At low current density, the difference is not obvious since even the lowest air flow rate (1.47 SLPM) corresponds to an excess coefficient higher than 4. At higher current densities, the difference becomes apparent. Since humidification of incoming gases was performed via the water collected in the humidifier at the downstream of cathode outlet, incoming gases to the stack were not fully humidified to 100% RH. Usually only 80% RH can be reached. This contributes to the low current density of current stack compared with a normal value, however not the major contributor. It should be noted that the final sharp drop of stack voltage at current density higher than

0.13 A/cm² was not attributed to the mass transport loss or dry out of membrane, which is usually the reason. Here the stack voltage of 2.4 V, for example, corresponded to three cells under normal operation and others “dead” (generating cell voltage lower than 0.1 V). In other words, it did not indicate that every cell was working at approximately 0.24 V, as one might suppose. That is to say, at high current density, one step increase of current to a certain level resulted several cells in the stack “dead”, although they were working properly at the previous current level. This is because at elevated current those (at least two) “dead” cells suffered from electrode flooding and the air flow was unable to remove liquid water that caused flooding. That is why at the maximum air flow rate (2.95 SLPM) such sharp voltage drop was not observed. Instead, the “dead” cell was generated one by one, noting every drop was roughly 0.8 V. Higher air flow rate is preferred in terms of better removal of water and prevention of flooding, therefore “dead” cell appeared gradually. This phenomenon will be further discussed in dynamic behavior section.

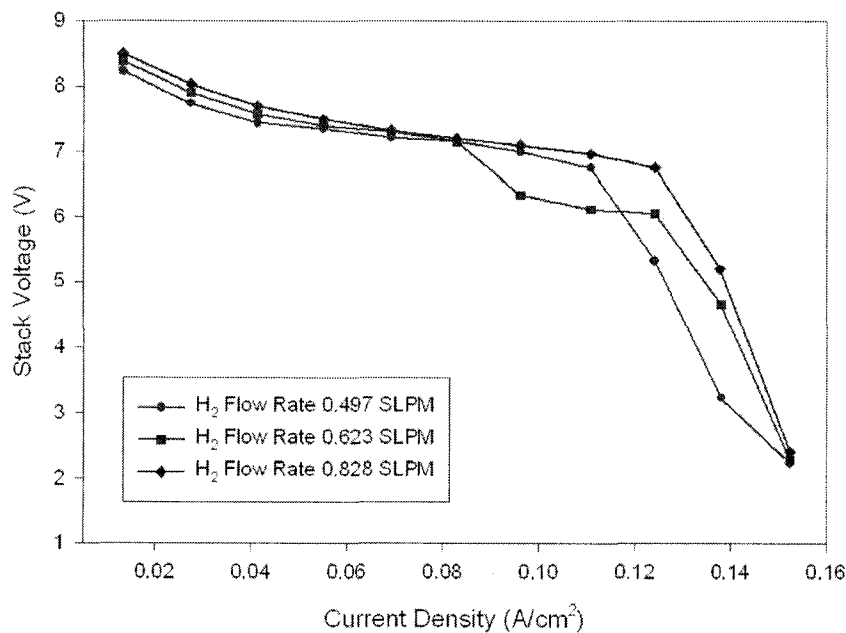


Fig. 8. Stack polarization curve under different hydrogen flow rates

Fig 26 shows hydrogen flow rate has very limited influence on the stack performance. Since hydrogen supply rate was sufficient to maintain the reaction, the stack voltage sharp drops observed in all cases were due to the “dead” cells at elevated current load. In other words, the stack performance was still determined by air flow rate. The same air flow rates resulted similar final stack voltage, i.e., three normally working cells.

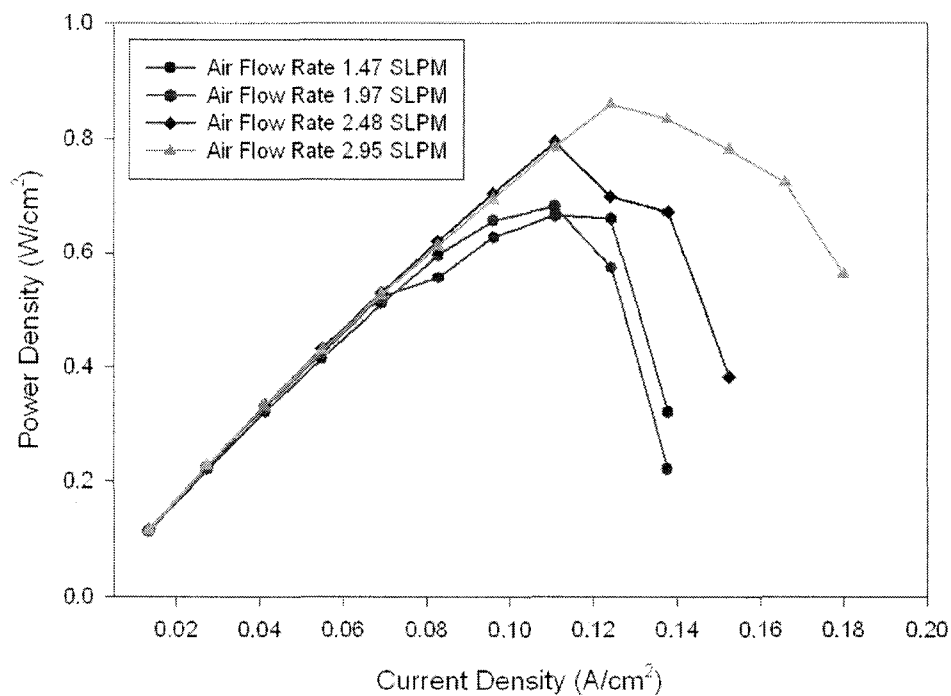


Fig. 9. Stack power output versus current density under different air flow rates

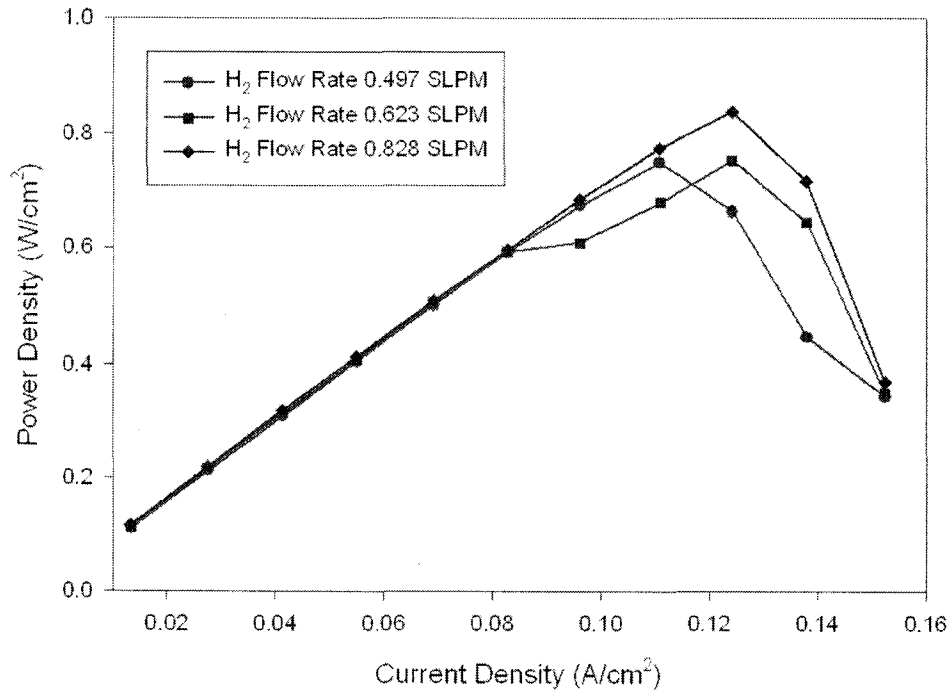


Fig. 10. Stack power output versus current density under different hydrogen flow rates

Figs 9 and 10 show the power output plots corresponding to Figs 7 and 8, respectively.

As expected, for both cases the power reached the maximum at a medium current that can be drawn from stack

4.2 Start-up cases

4.2.1 Stack voltage responses

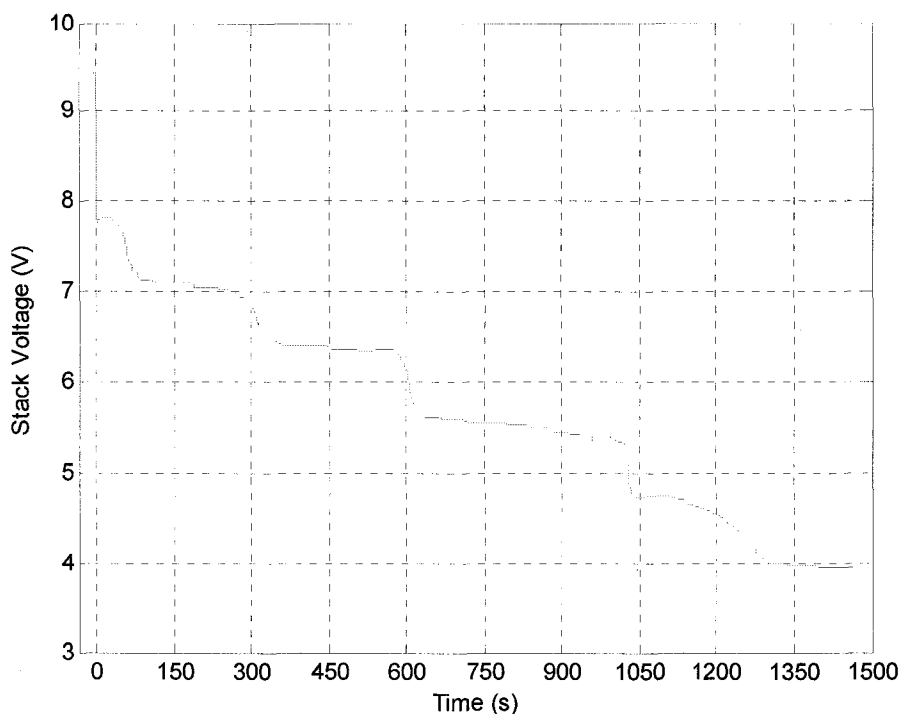


Fig. 11. Stack voltage response when stack started from idle to 1 A load

Fig. 11 shows how the stack voltage changed with time when the stack started to 1 A load. The air flow rate was low due to the low current load of 1 A (excess coefficient fixed for all start-up cases). With the reaction moving forward, more and more water was generated but not removed smoothly due to the unknown problems in gas channel design and fabrication and the low air flow rate. In addition to humidify the membrane, liquid water accumulated and then flooded the electrode. Gradually, more and more cells became “dead” and stack voltage was observed to experience sudden sharp drop when one more malfunctioned. Because of the low air flow rate, or, its low capacity to remove liquid water, “dead” cells cannot recover. When there were only five cells working, the stack voltage appeared to stop decreasing, or, no more cells became “dead”. This indicated that besides the electrodes, cathode gas channels in those non-working cells

may have been also blocked by liquid water so that air can hardly pass through those cells.

The average air flow rate at the channels of the remaining five cells was therefore increased, which explains why these cells no longer suffered from electrode flooding.

Finally, the stack voltage (five working cells) was observed to be stable.

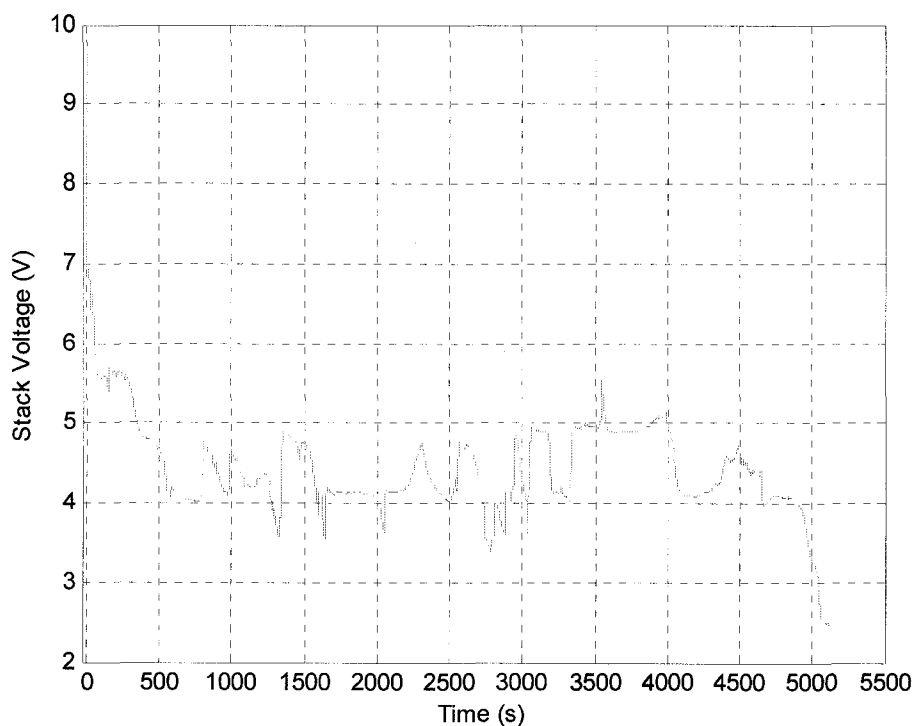


Fig. 12. Stack voltage response when stack started from idle to 2 A load

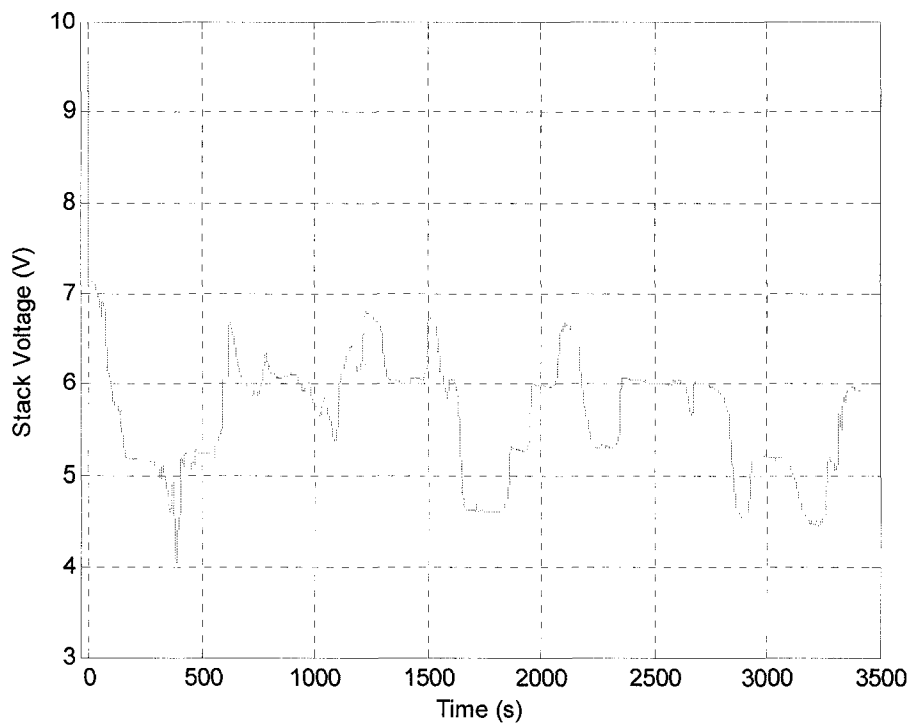


Fig. 13. Stack voltage response when stack started from idle to 4 A load

Figs 12 and 13 presented obvious voltage oscillation compared with Fig 11. At an elevated current load, the air flow rate was higher given the same excess coefficient. The reason for oscillation is that the air flow rate was not high enough so that several (not all) cells can be maintained always without flooding; whereas the air flow rate was high enough so that if too many channels were blocked by water (total gas channel cross section area reduced and average air flow rate increased), one or two “dead” cells can recover when liquid water in gas diffusion layer/channel being removed by air flow. The non-working cell during the oscillation may be arbitrary based on the observation in experiments, one newly flooded cell may result another one that was previously “dead” to recover. This can be attributed to the fact that although the average air flow rate was

increased, it is arbitrary to determine the water in which cell was firstly removed. As soon as water in one cell's channel was removed, the average flow rate reduced and probably no additional cell can further recover due to insufficient air flow rate.

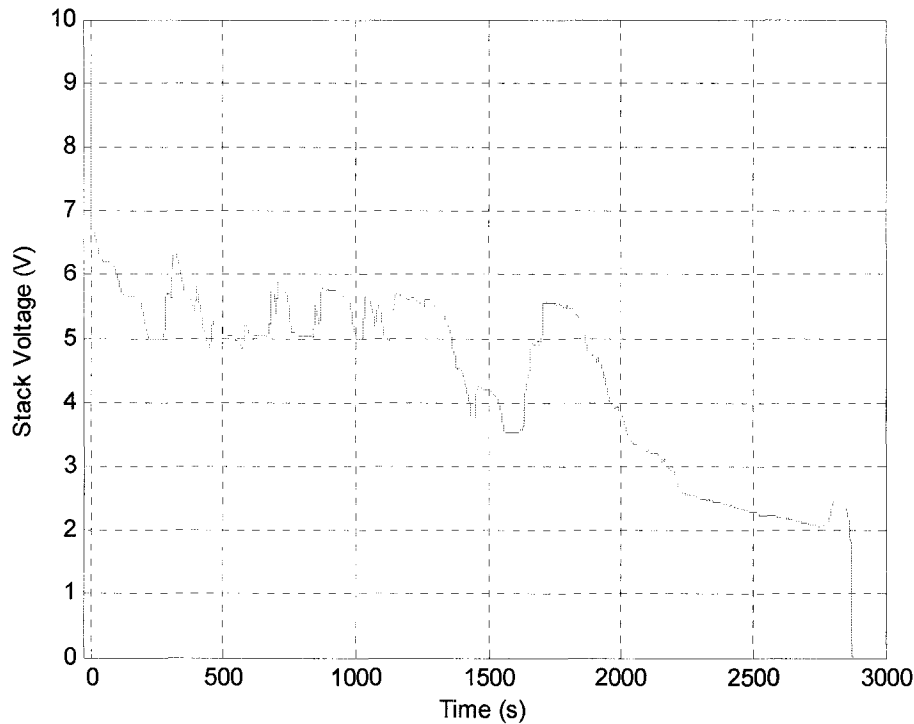


Fig. 14. Stack voltage response when stack started from idle to 6 A load

As shown in Fig. 14, the stack voltage response from idle to 6 A load was similar to previous cases except that finally the stack voltage fell down to zero, all cells being flooded to “dead”. The final drop began at around 1800 seconds after start-up. The water generation rate at cathode was very high at and after that moment since the current was high and the stack temperature had already reached the optimum level. A great amount of water flooded all cells at a high speed such that it was no longer removable by increase of air flow rate at remaining open channels. Finally all cells became non-working.

4.2.2 Temperature responses

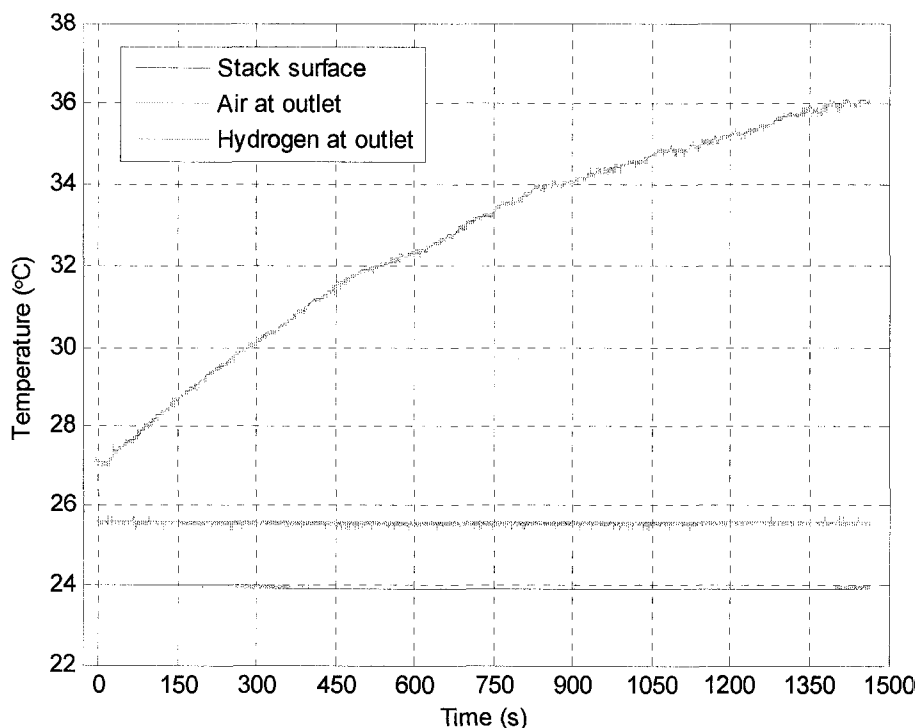


Fig. 15. Change of temperature with time when stack started from idle to 1 A load

As shown in Fig. 15, the stack surface temperature increased with time slowly due to the low current level. Air/Hydrogen temperature at outlets was measured by thermistor/thermocouple mounted at the outlet fittings, heat contained in the reactant gases were quickly dissipated to the stainless steel fittings before reaching the thermocouple. Therefore small amount of heat was insufficient to increase the temperature readings from thermocouples. This explains why air/hydrogen temperature readings at outlets remained almost unchanged in this case. Additionally, at the cathode outlet, there was always some liquid water (could be the water remained in system since

previous operation) condensed at the thermistor surface, which resulted the lower temperature reading at cathode outlet. In other words, air may not fully contact the thermistor surface and its reading was be influenced by previously condensed water. However, this problem may be difficult to resolve since the cathode outlet environment always contains a great amount of liquid water, generating error in gas temperature measurement.

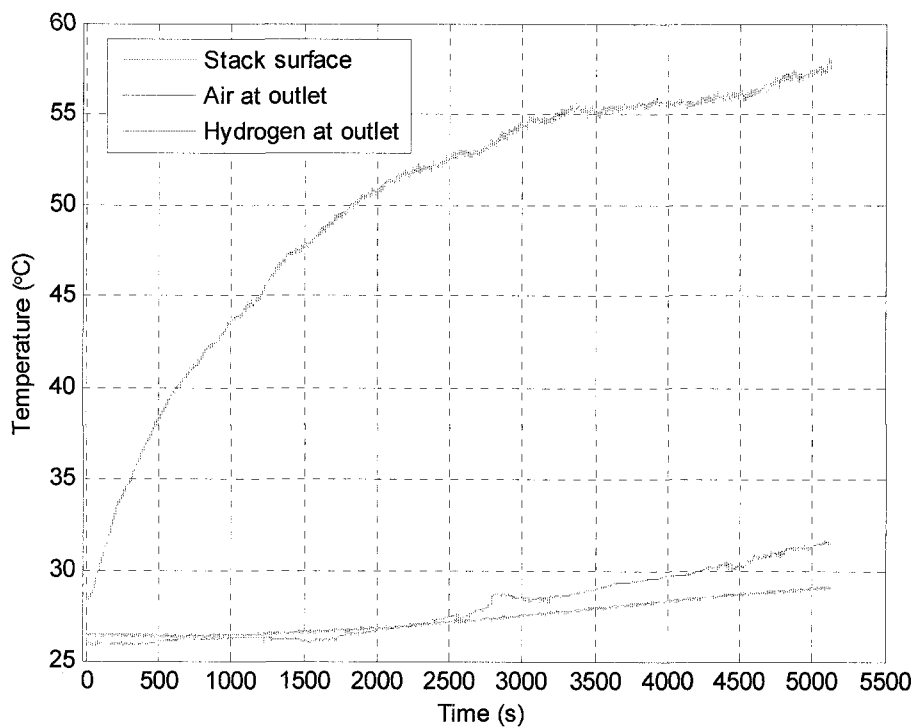


Fig. 16. Change of temperature with time when stack started from idle to 2 A load

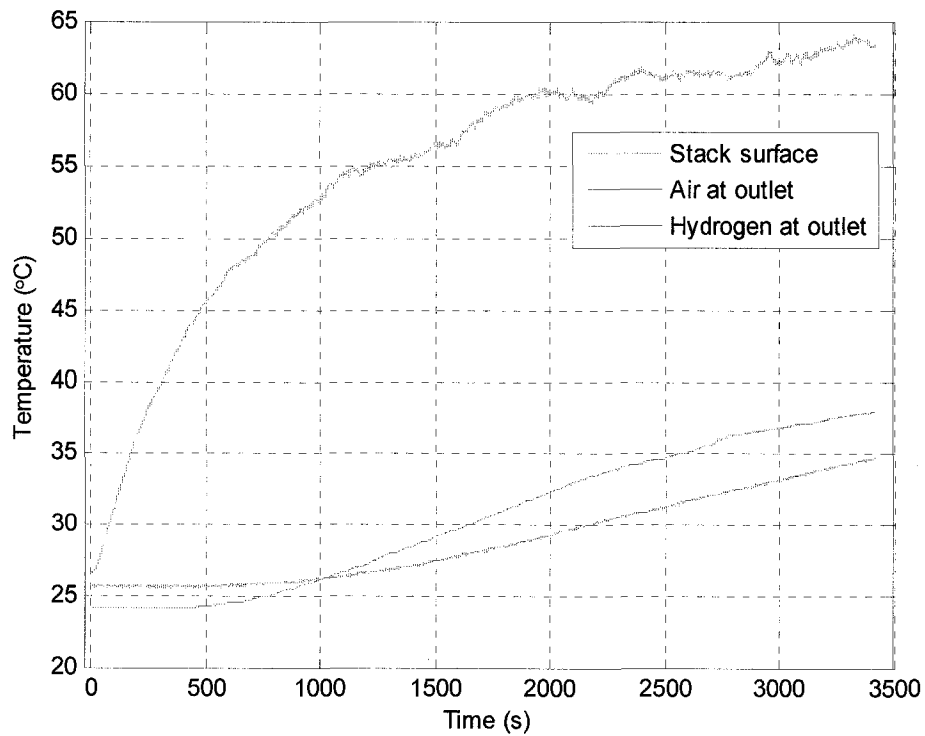


Fig. 17. Change of temperature with time when stack started from idle to 4 A load

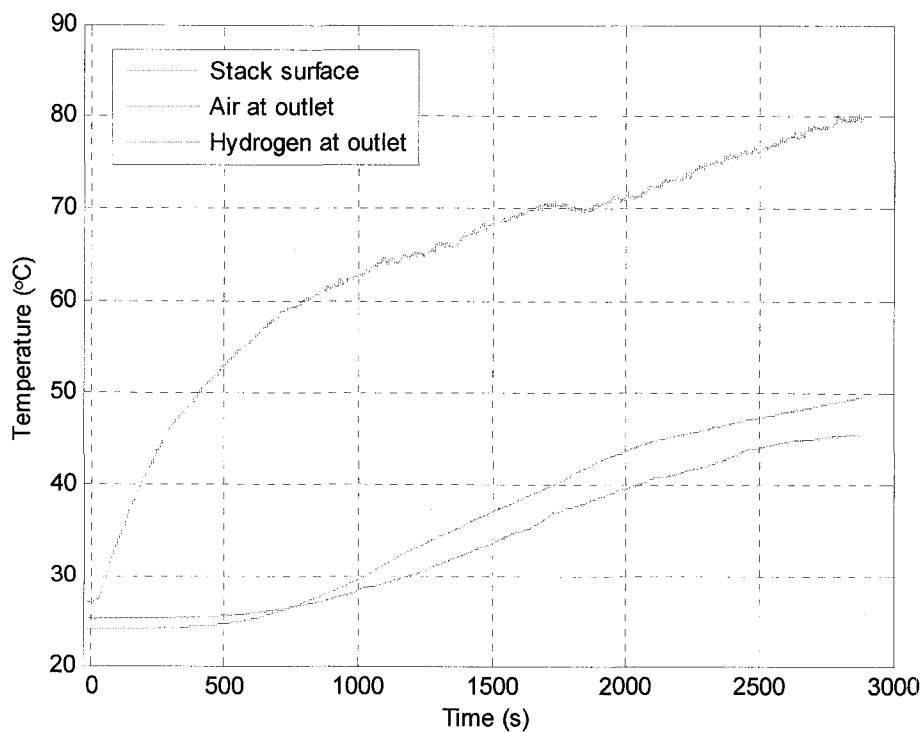


Fig. 18. Change of temperature with time when stack started from idle to 6 A load

As shown in Figs 16, 17 and 18, at an elevated current load, all three temperatures measured experienced an apparent increase with time. Higher current load saw a quicker temperature increase. The stack temperature moved into the optimum range at around 3000, 1500 and 800 seconds after start-up respectively. The air temperature at outlet surpassed the hydrogen temperature after a certain period of operation, both showing obvious trend of increase in the meantime. This due to the fact that reaction at cathode releases much more heat compared with anode, which is dominant over the influence of condensed water on the thermistor surface as mentioned. On the other hand, the stack itself became very hot at elevated current, which also heated the gases passing through. Still, part of the heat was lost at internal surface of outlet fittings, however the remaining was sufficient to raise the reading of sensors.

4.2.3 Pressure drop responses in time domain

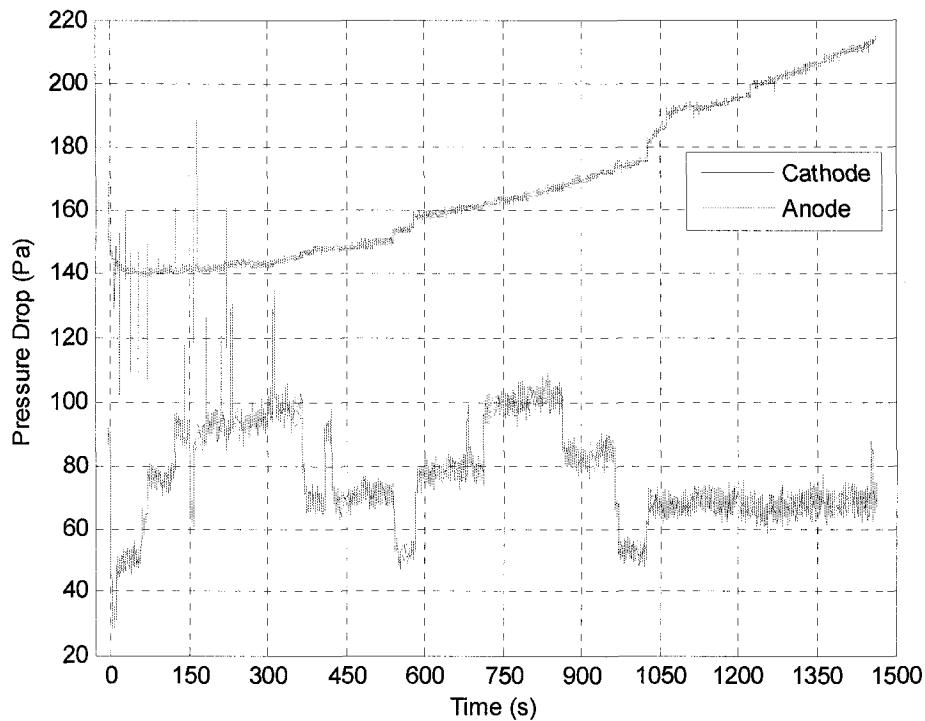


Fig. 19. Change of pressure drop with time when stack started from idle to 1 A load

Fig. 19 shows the cathode (air)/anode (hydrogen) pressure drop changes when the stack started to 1 A load. The cathode pressure drop kept increasing since the average air flow rate at opening channels was increasing when more and more channels became blocked and cells became “dead”. It is supported by the fact that the relatively abrupt increase of cathode pressure drop at around 600 and 1050 seconds corresponds to stack voltage drop at the same time in Fig 27. For anode pressure drop, besides those numerous small oscillations, which will be explained later, there are several large and apparent oscillations, as one can see before 600 and 1050 seconds. Again, such undershoots relates to the stack voltage drop at that time. Because new “dead” cells appeared at those moments due to cathode electrode flooding, the hydrogen consuming rate, or, the rate

hydrogen ion generation at the catalyst sites was reduced before those moments. Time delay between stack voltage drop and decrease of anode pressure drop can be explained as follows: when the cathode gas diffusion layer was blocked by water, there was a certain amount of air left at the catalyst layer, which can still sustain the reaction for a while. Hence the stack voltage would not fall down immediately. However, as soon as gas diffusion layer was blocked, the reaction rate at cathode catalyst layer was reduced since oxygen was not replenished any longer; thereby reducing hydrogen ion concentration gradient in the membrane (unconsumed hydrogen ion accumulated). As a result, reaction that hydrogen was oxidized to hydrogen ion at anode catalyst layer would become much slower. Hydrogen flow passed through the electrode without or with much less consumption, consequently the anode pressure drop reduced abruptly. Furthermore, the immediate increase of anode pressure drop after undershoot was attributed to the back diffusion of liquid water to the anode, which even flooded the anode. Liquid water in anode gas diffusion layer and/or channel would hinder the hydrogen flow, thereby increasing the pressure drop. Finally, the author would like to address the abrupt increase of anode pressure drop right after 300 seconds, which corresponds to the stack voltage drop at that time. Note that cathode pressure drop did not experience abrupt increase at around 300 seconds, which means this stack voltage drop started from the anode flooding instead of cathode. It seems to be unusual but considering the stack had just started for five minutes, liquid water resulting anode flooding may be remaining water in the system after previous operation.

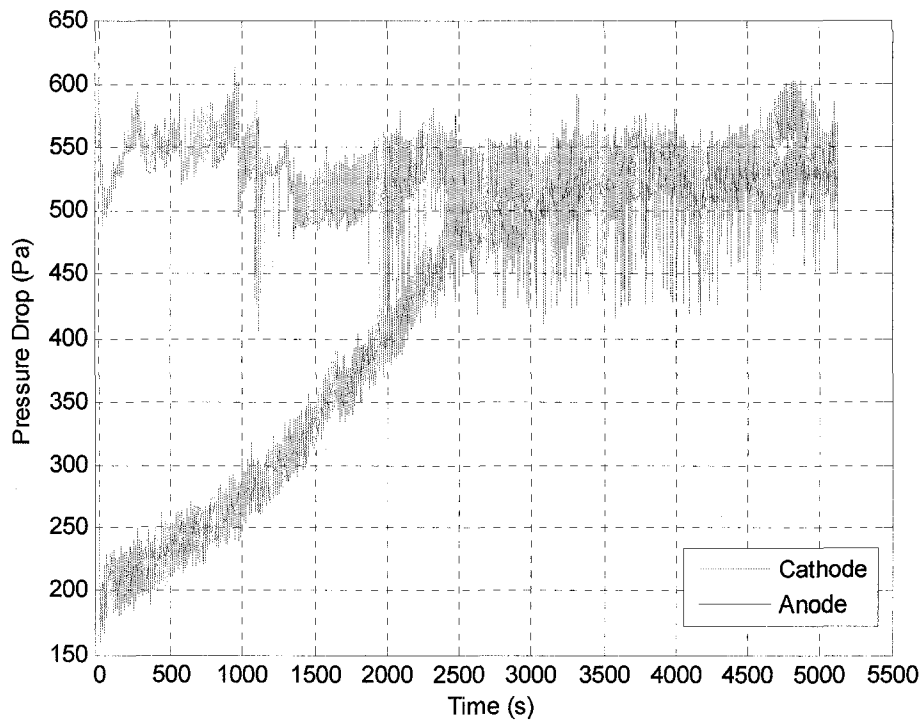


Fig. 20. Change of pressure drop with time when stack started from idle to 2 A load

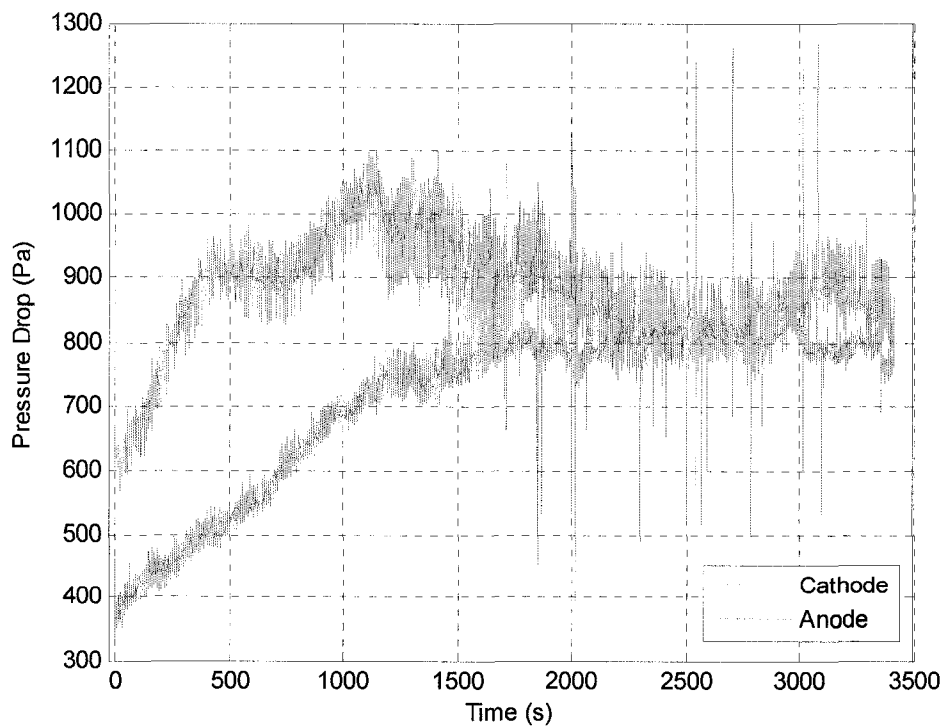


Fig. 21. Change of pressure drop with time when stack started from idle to 4 A load

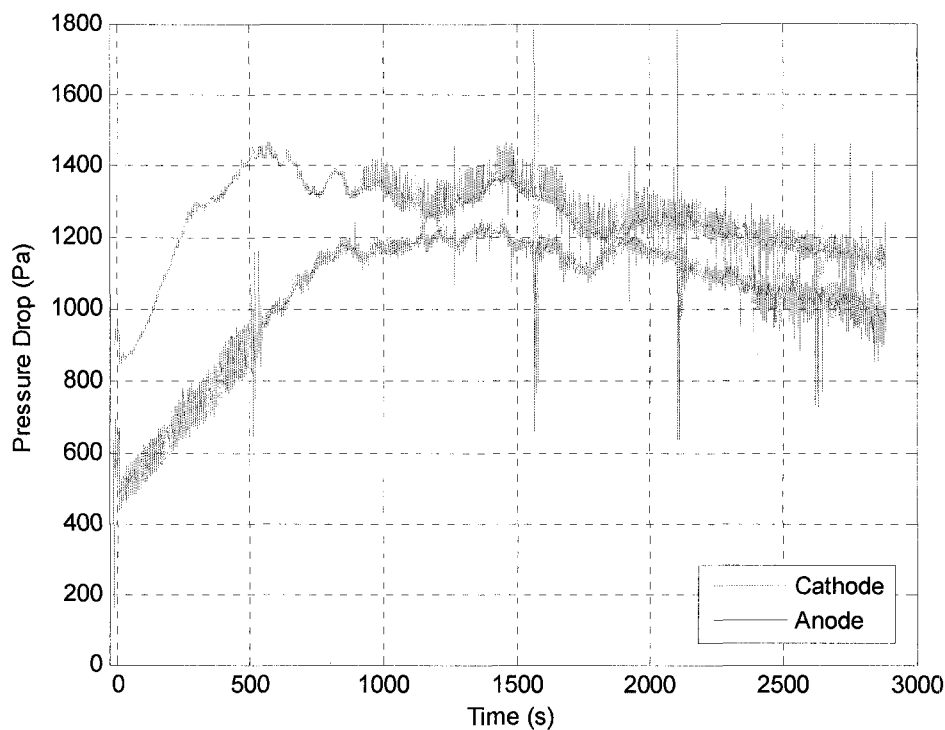


Fig. 22. Change of pressure drop with time when stack started from idle to 6 A load

Figs 20, 21 and 22 show the pressure drop changes when the stack started to higher current loads. The pressure drop signals in these cases contain too much high-frequency, high-peak oscillation compared with Fig 15 (notice the pressure drop axis scale). Therefore, unfortunately such signal can hardly be analyzed in a time domain, much information being masked by oscillation. Essentially, the high-frequency oscillation was due to the liquid water in the system. At elevated current, much more water would be present and the reactant flow was disturbed more arbitrarily and frequently. Overall, such signal can still be analyzed without too many details. For example, in Fig 16 the anode pressure drop increased with time before 4000 seconds due to the increase of water amount at anode, experienced an undershoot at around 4000

seconds due to the “dead” cell generated at that time, just as explanations for the case of start-up to 1 A load. However, such overall analysis is insufficient.

4.2.4 Dominant frequencies of pressure drop signals

To combat this problem, the author turned to frequency domain, aiming to find the relationship between pressure drop and stack voltage. Signals are converted from time domain to frequency domain usually through the Fourier transform. It converts the signal information to a magnitude and phase component of each frequency. Customarily the Fourier transform is converted to the power spectrum, which is the magnitude of each frequency component squared. The most common purpose for analysis of signals in the frequency domain is analysis of signal properties. The spectrum can be studied to obtain information of which frequencies are present in the input signal and/or which are significant component.

A fast Fourier transform (FFT) is an efficient algorithm to compute the discrete Fourier transform (DFT). For the pressure drop signal, it was sampled every 0.16 second and recorded in the data file. Therefore it can be considered a discrete data sequence and FFT can be performed, although the pressure drop itself was analog signal.

Let x_0, \dots, x_{N-1} be complex numbers, the DFT is defined by the following formula:

$$X_k = \sum_{n=0}^{N-1} x_n e^{-\frac{j2\pi}{N}nk} \quad k=0, \dots, K-1$$

Obviously, this algorithm is complicated to work out as it involves many additions and multiplications of complex numbers. FFT is another method for calculating the DFT. While it produces the same result, it is incredibly more efficient, often reducing the computation time by hundreds. The details of FFT algorithm is not presented here as in the study it was performed simply by related Matlab commands without knowing the internal workings.

To process the pressure drop data through FFT technique, the author would like to first introduce two self-defined parameters. “Window” is the data to be together processed by FFT. For every start-up case, the duration is at least 1500 seconds; every 0.16 second there is a pressure drop data, totally amount of data is therefore tremendous. One needs to determine how many data to be processed one time so that the optimum power spectrum that facilitates analysis can be generated. The amount of data is termed “window size”. In Matlab codes developed for processing pressure drop data using FFT, the author applied the algorithm that in every consecutive seven data, take the first one as the “window center”, that is, half of the window size applies to the data right before the center and half to after the center. In this way that point of data becomes the center of the window. Taking first data out of every consecutive seven ones as the window center is to separate window centers by 0.96 second, roughly one second (time between two consecutive data is 0.16 second). At each window center, grab data identically (half window size) before and after to form one FFT processing object.

The power spectrum obtained after performing FFT on the window will have numerous frequency components that show different power. The frequency having maximum power obviously is the major component. However considering only the frequency at maximum power may not be reasonable especially when the second maximum power is very close to the maximum. Here the author defines a parameter to describe the major frequency component, which is of most significance in the pressure drop signal.

$$\text{Normalized Dominant Frequency} = f_1 \times \frac{P_1}{P_1 + P_2 + P_3} + f_2 \times \frac{P_2}{P_1 + P_2 + P_3} + f_3 \times \frac{P_3}{P_1 + P_2 + P_3}$$

where P_1 is the maximum power and f_1 the corresponding frequency, P_2 , P_3 the second and third maximum power and f_2 , f_3 the corresponding frequency.

The Normalized Dominant Frequency indicated the major frequency component by taking the largest three powers and corresponding frequencies into account.

Starting from zero, window centers are located at the beginning of every 0.96 second, where FFT were performed given a specific window size. However, the window size cannot be applied to all window centers from zero to end. If the half of the window size is larger than the amount of all available data between the zero and window center, for example, the time for the window center is 0.96 second after start-up whereas the half window size is 20 data, which corresponds to $20 \times 0.16 = 3.2$ s, then the half window size changes to the amount of all data between zero and window center, with window size doubled. This algorithm also applies if the window center is approaching the end of time

period for data recording, i.e., if the half window size is larger than the distance between end of time period and window center in terms of amount of data/time, the distance between automatically becomes the half window size.

Now the plot of time versus normalized dominant frequency can be obtained at a time step of 0.96 second. Algorithms mentioned above and the plotting was performed by Matlab codes. It should be noted that such plot is not unique since the window size has not been specified. Different window sizes may generate different plots. The procedure for determining a suitable window size is introduced as follows.

The author would like to first calculate the time for air/hydrogen to pass the gas channels in the stack at a given mass flow rate or current load. Two assumptions in this approximate estimation are: 1) no water in the channel, i.e., dry gases passing dry channels; 2) no velocity loss at the turns of serpentine channels. Following formula was used:

$$\text{Time to pass channel (s)} = \frac{\text{Mass flow rate (mm}^3/\text{s)}}{\text{Cross section area of channel (mm}^2) \times \text{number of channels} \times \text{channel length (mm)}}$$

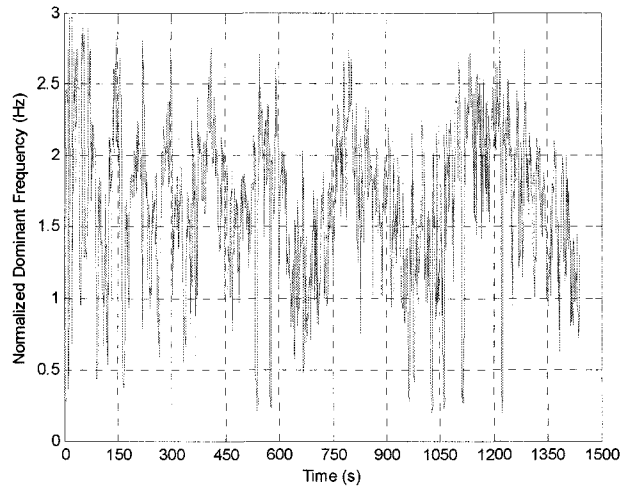
where the channel length was calculated by length of straight part multiplying number of serpentine turns; number of channels was calculated by number of parallel channels in one cell multiplying number of cells in the stack. All specification data in calculation were from Palcan Power Systems Inc. Results are presented in the table below.

Current (A)	Hydrogen flow rate (L/Min)	Air flow rate (L/Min)	Time to pass the anode channel (s)	Time to pass the cathode channel (s)
1	0.09	0.34	4.5864	2.2258
2	0.17	0.67	2.4281	1.1295
3	0.26	1.00	1.5876	0.7568
4	0.34	1.33	1.2140	0.5690
6	0.51	2.00	0.8094	0.3784
Excess coefficient for hydrogen is 1.2, for air 2. Cross section area for anode is 0.78 mm^2 , for cathode 1.43 mm^2 . Number of parallel channels in one cell is 2; number of cells in the stack is 10. Length of straight part in serpentine channels is 63 mm; number of serpentine turns is 7 mm.				

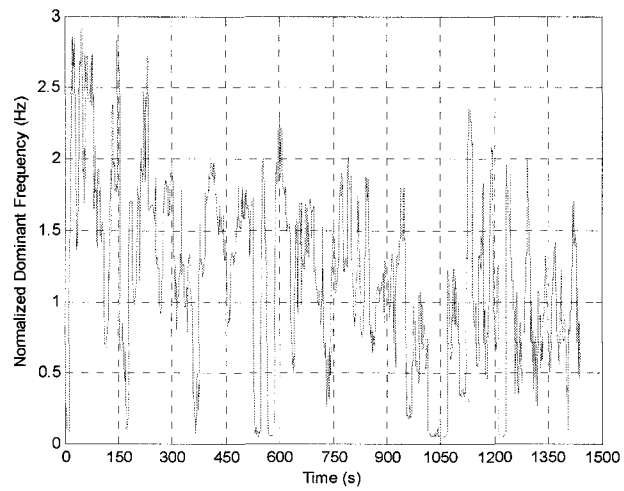
Table 3. Channel specifications and time to pass channel at different current loads

Time values in Table 3 divided by a factor of 0.7 can be regarded as the time to pass channel when water is present, multiple of which may be used as a suitable window size. Although it is an approximate estimation, a series of multiples can be tried and compared to find the optimum window size. The reason for choosing time to pass channel as the base for window size selection is that such parameter relates to the frequency of water removal from the channel, if the reactant flow is able to bring some water away. In this way the author believes the relationship between dominant frequency of pressure drop signal and stack voltage can be revealed more easily.

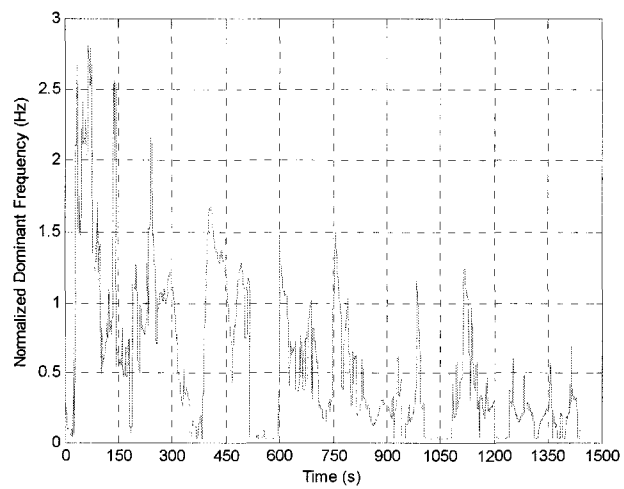
To show how to select the optimum window size, take an example of start-up to 1 A case. Dominant frequency of cathode pressure drop versus time plots are presented in terms of different window sizes:



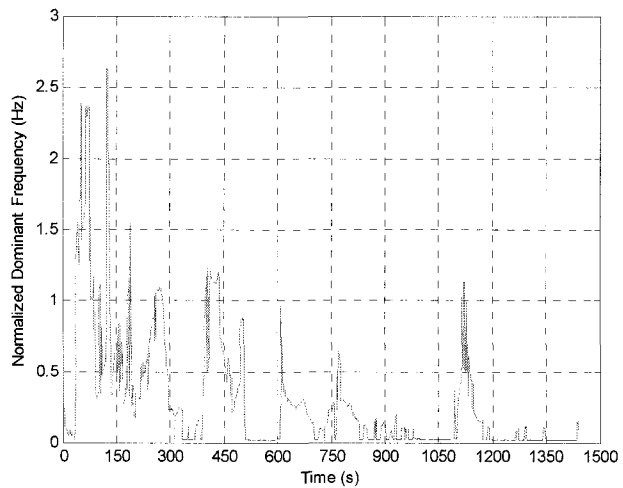
Window size 36 data, or 5.76 seconds



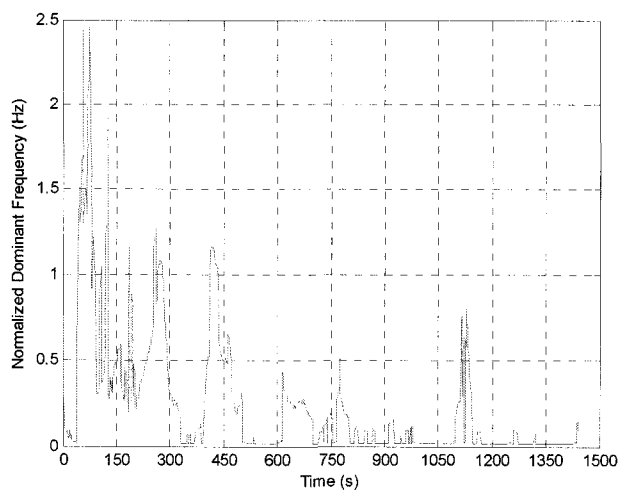
Window size 144 data, or 23.04 seconds



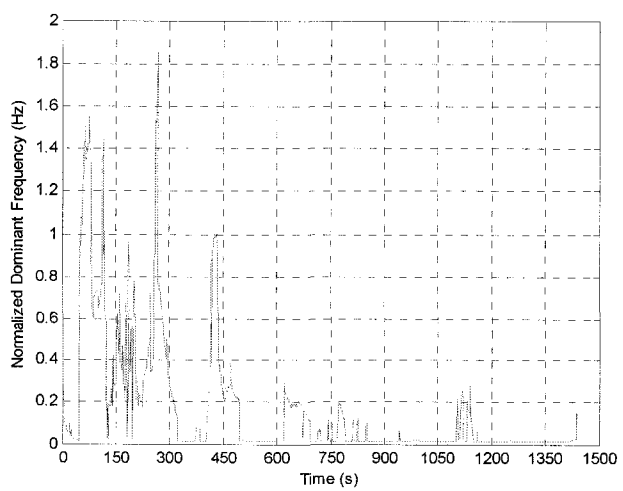
Window size 288 data, or 46.08 seconds



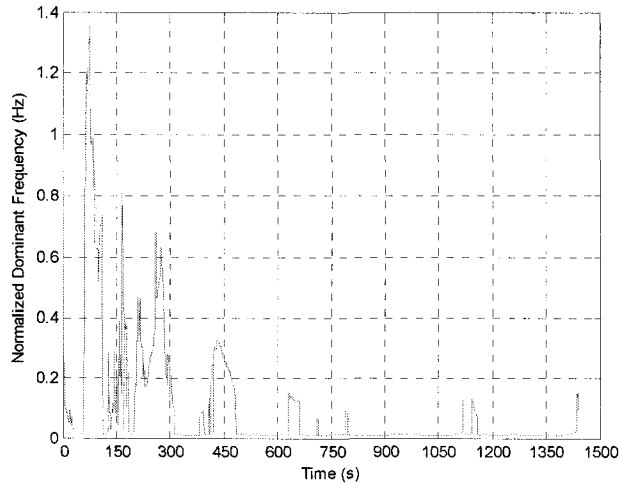
Window size 432 data, or 69.12 seconds



Window size 504 data, or 80.64 seconds



Window size 576 data, or 92.16 seconds



Window size 720 data, or 115.20 seconds

Fig. 23. Dominant frequency versus time plots under different window sizes

First, it should be noted that the maximum frequency does not exceed 3.125 Hz, which is half of the sampling frequency of the pressure drop data ($1/0.16=6.25$ Hz). Such maximum frequency is also called Nyquist frequency in FFT algorithm. This relationship has to be followed for performing FFT. The normalized dominant frequency calculated by the largest three frequency components is obviously within the same range.

Revisit Fig 11 for stack voltage response and compare with plots in Fig 23. As shown, too small window size will result unwanted noise or oscillation so that useful information is still masked, whereas too large window size will reduce frequency peaks and remove some relatively low peaks, which may be a loss of important information. A medium window size, which is 504 data in this case, is the optimum, all major peaks being shown but hardly noise. The criteria for window size selection can be summarized as:

- 1) Show less noise (unless the oscillation cannot be removed even with a large window size, which means dominant frequency does oscillate with time);
- 2) Retain significant peaks, especially those that are potentially correlated with stack voltage increase/decrease;
- 3) Small window size is preferred if above two being satisfied simultaneously, because small window size means less delay if feedback control is performed to stabilize the stack voltage. Also, small window size results larger frequency peaks that are retained, which is preferred by testing instrument.

The above criteria apply to dominant frequency plots in all start-up and current step-up cases. However, for other cases, only the plot generated under the optimum window size is presented, i.e., the comparison and selection process will no longer show due to the limited space. Following figures put together the dominant frequency and stack voltage plots with time. As mentioned, the purpose is to establish the relationship between pressure drop frequency and stack voltage, which is not so clear if pressure drop signal analyzed in only time domain. Instead, pressure drop signal was first processed in frequency domain to obtain the dominant frequency. This frequency is believed to correlate with stack voltage response during start-up. The author would like to also emphasize that the dominant frequency does not mean the physical changing frequency of the pressure drop signal; it only indicates the major frequency component of a series of samples. The focus of study is the relative trend of frequency change and not individual frequency values, which is variable over different window sizes and sampling rates.

4.2.4.1 Dominant frequency of cathode pressure drop versus stack voltage

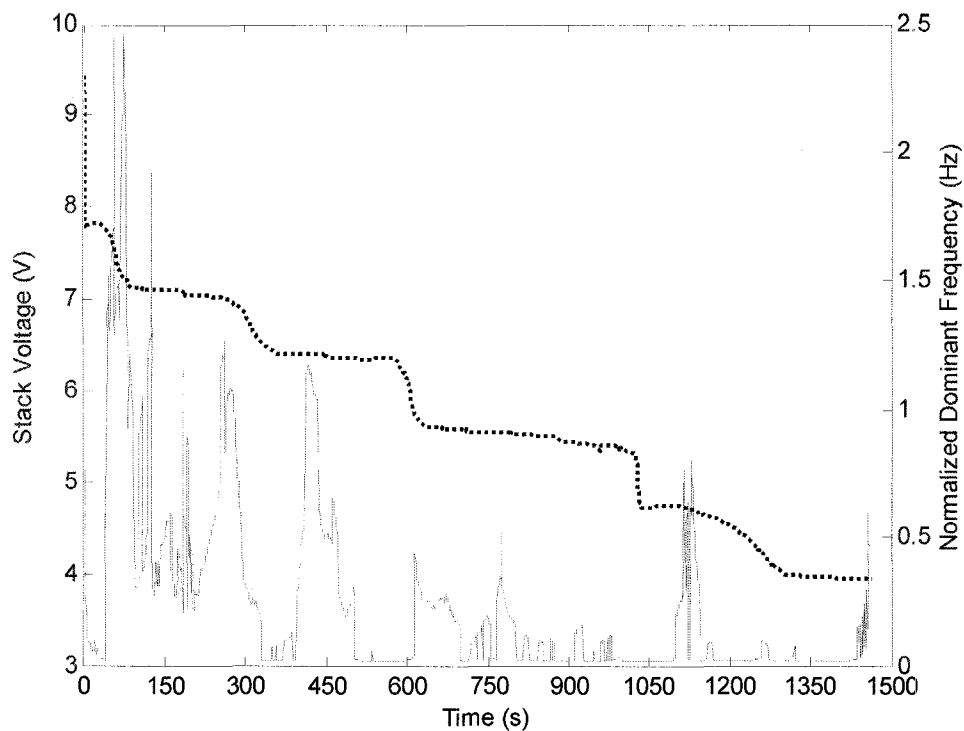


Fig. 24. Changes of dominant frequency of air/cathode pressure drop and stack voltage with time when stack started from idle to 1 A load

As shown in Fig 24, when stack started from idle to 1 A load, the stack voltage drop, or, generation of “dead” cell was predicted by one or several frequency peaks before. Frequency peaks indicated that the water began to flood the gas diffusion layer and gas channel. Air flow was disturbed and pressure drop became unstable, as can be found around 450 seconds. Then the frequency became almost zero, which means air no longer passed through this flooded cell. However, the stack voltage remained for a while, because 1) the air left in electrode can sustain the reaction for a while at low current; 2) small voltage reduction in this flooded cell was compensated by voltage increase of other

cells under a higher average air flow rate. After 600 seconds another cell began to suffer flooding, which caused the unstable pressure drop again. For this cell, it took a longer time to be fully flooded, a series of frequency peaks being the evidence. The abrupt stack voltage drop also appeared later than frequency becoming almost zero. Again, although the air did not pass the flooded cell, its cell voltage saw a gradual decrease at first and then the abrupt drop after a while. Both the frequency peak and flat bottom can be used as the diagnosis tool for in-process flooding and cease of air flow to the flooded cell, respectively. It should be addressed that the initial and final frequency peaks are due to the algorithm regarding the window size. Also, there may be some liquid water left in the stack that caused the frequency peaks before 150 seconds. The system was always unstable at initial start-up due to the low stack temperature and liquid water left inside since previous operation. As a result, frequency plot at the beginning and end may be ignored.

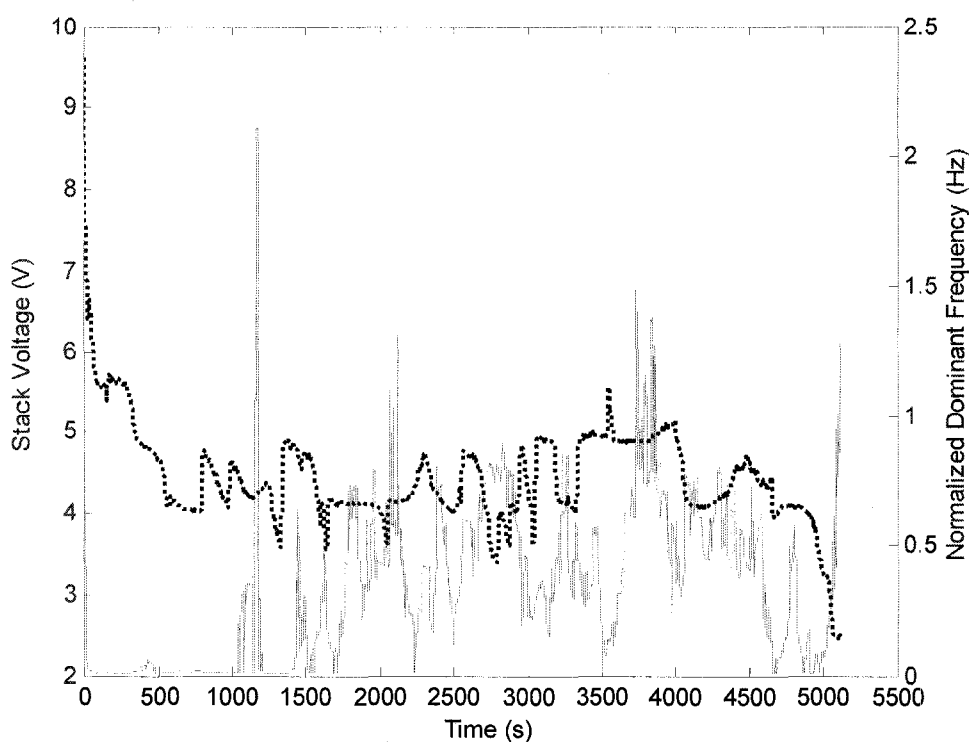


Fig. 25. Changes of dominant frequency of air/cathode pressure drop and stack voltage with time when stack started from idle to 2 A load

As shown in Fig 25, frequency change with time at 2 A load start-up was much more complicated. Initial flat bottom of low frequency was attributed the increased air flow rate in this case, which may be capable to remove the remaining water in the channels very soon. On the other hand, fresh water generated via reaction was too few to influence the air flow at initial start-up. Consequently the pressure drop was relatively stable for approximately 1000 seconds. The initial stack voltage drop was due to the time delay of mass transport to the catalyst layer and low stack temperature.

After 1000 seconds, the frequency began to oscillate. Every peak corresponds to the in-process flooding in gas diffusion layer and channel. As mentioned before, stack voltage oscillation was because that air flow was capable to remove water in one or two flooded cells if too many cell channels were blocked. Therefore, the bottoms of frequency oscillation were the indication that one or two cells that were flooded previously now recovered after water was removed. Notice the stack voltage and dominant frequency signals from 2000 seconds to 3500 seconds approximately, these two signals present a roughly 180 degree phase delay relationship if modeled by a sine function, i.e., the peak of stack voltage corresponds to the bottom of frequency and vice versa. Water flooding-removal cycle essentially determined the phase reverse of these two signals. In this case again, a stable stack voltage with one or several simultaneous frequency peaks predicted an abrupt voltage drop after a period for time.

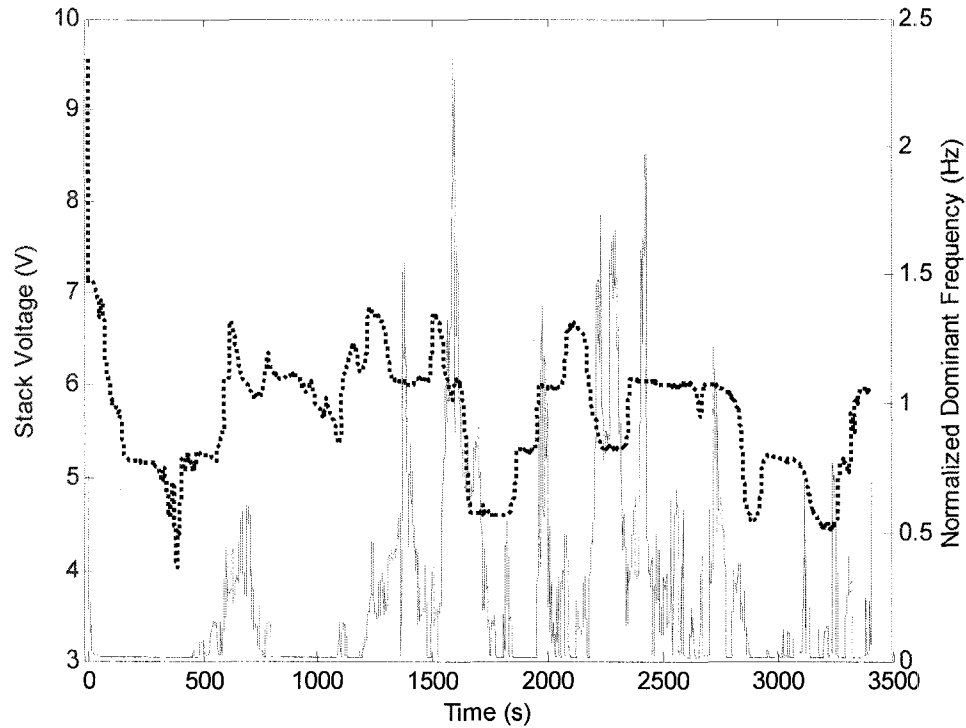


Fig. 26. Changes of dominant frequency of air/cathode pressure drop and stack voltage with time when stack started from idle to 4 A load

Fig 26 shows that in 4 A start-up case, the frequency oscillation also happened with even more higher peaks. This can be explained by the fact that at 4 A load, more water was generating, imposing more disturbance on the air flow. Again, the reverse phase of stack voltage signal and frequency signal was observed.

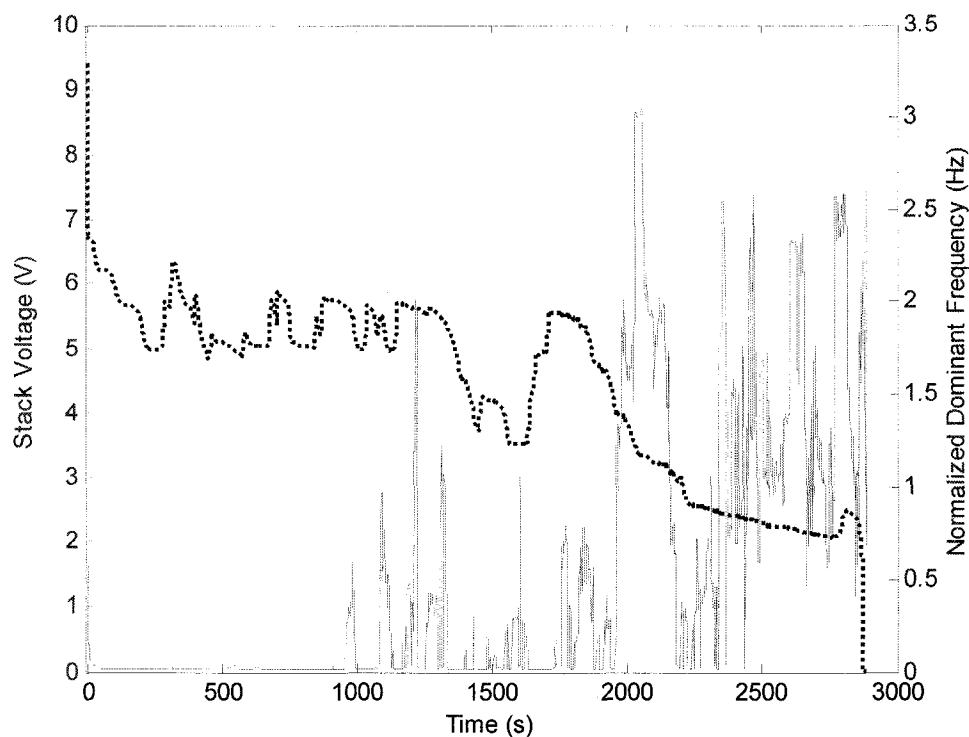


Fig. 27. Changes of dominant frequency of air/cathode pressure drop and stack voltage with time when stack started from idle to 6 A load

As shown in Fig 27, initially it took almost 1000 seconds for frequency starting to oscillate. This is because, at 6 A load the air flow rate was high (2 SLPM), small amount of water was readily removed and cannot disturb the air flow until the reaction rate increased with stack temperature, sufficient water being capable to flood the cell. The stack voltage oscillation before 1000 seconds may be related to the unstable and uneven mass transport, since there was still certain amount of water, either freshly generated or previously left, in the gas diffusion layer. Here it is shown again that initially after start-up, the frequency information may not be well utilized as a diagnosis tool for stack voltage. In this case, finally the stack voltage fell to zero and the load was shutdown

owing to the flooding in all cells. During the final voltage drop to zero, frequency saw a series of intense oscillations obviously due to the great amount of water in the channel. The air flow still passed the stack, probably through several cells whose channels were not fully blocked, but being highly disturbed by water and unable to reach the catalyst layer.

4.2.4.2 Dominant frequency of anode pressure drop versus stack voltage

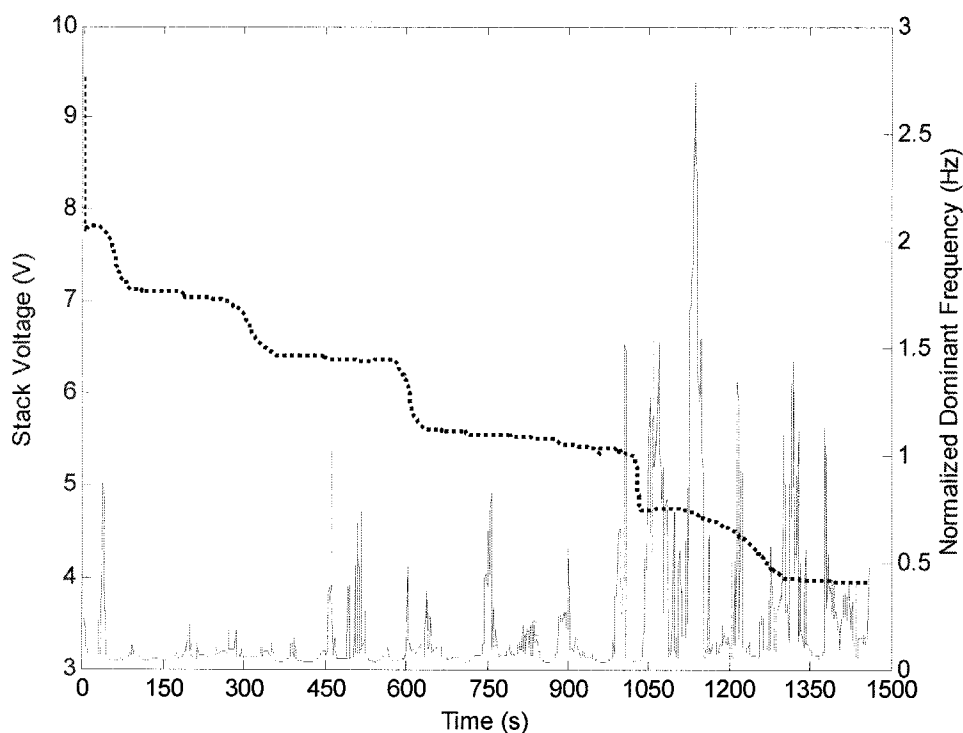


Fig. 28. Changes of dominant frequency of hydrogen/anode pressure drop and stack voltage with time when stack started from idle to 1 A load

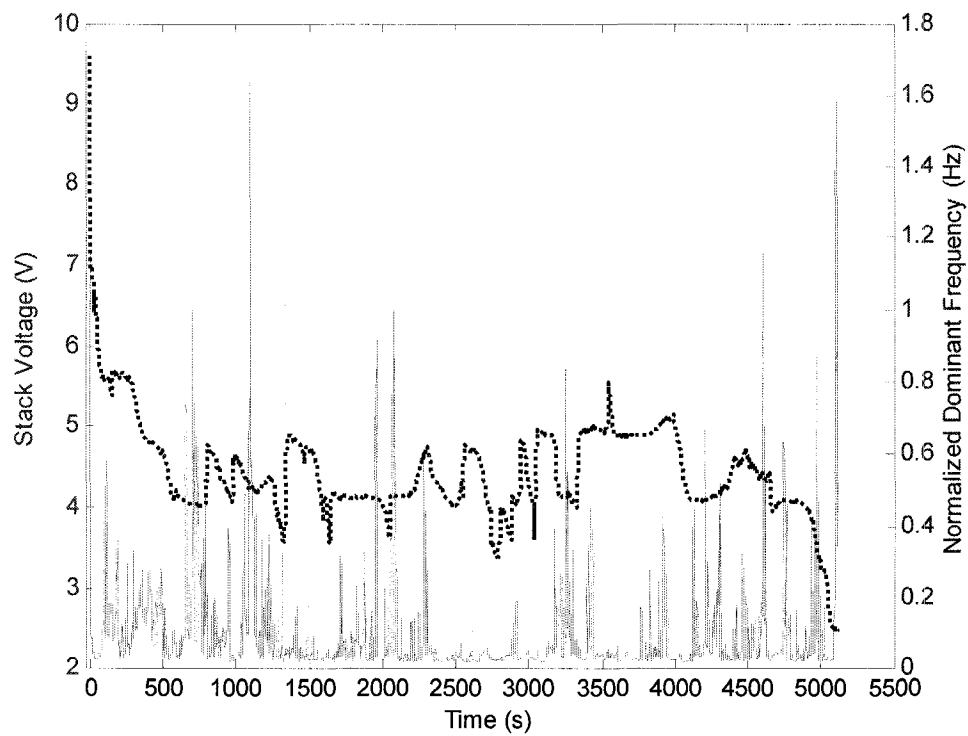


Fig. 29. Changes of dominant frequency of hydrogen/anode pressure drop and stack voltage with time when stack started from idle to 2 A load

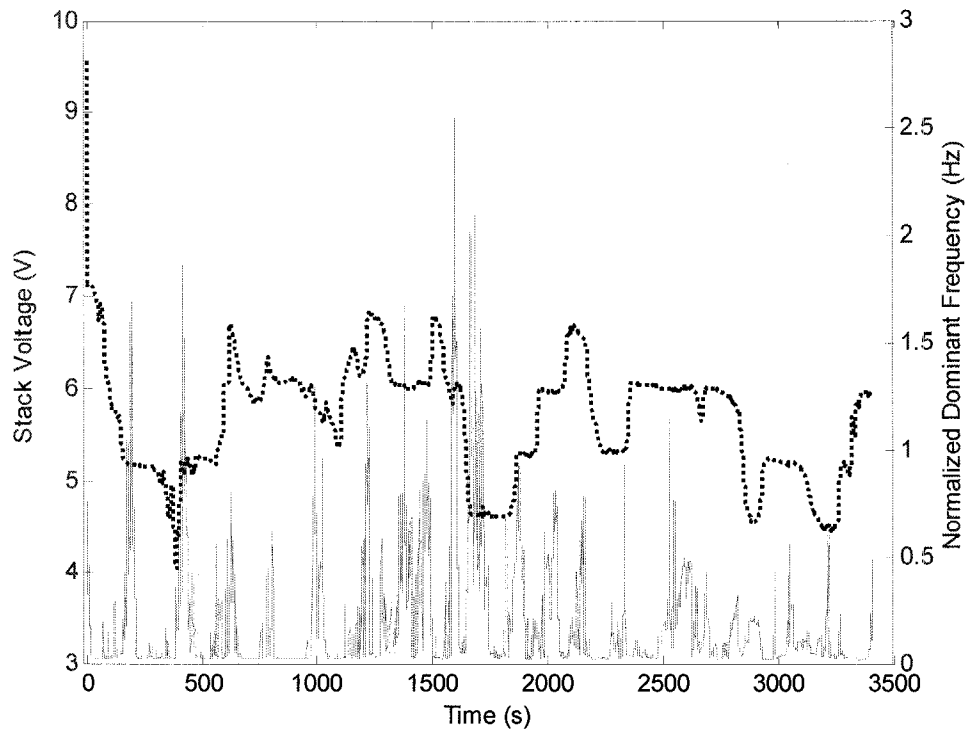


Fig. 30. Changes of dominant frequency of hydrogen/anode pressure drop and stack voltage with time when stack started from idle to 4 A load

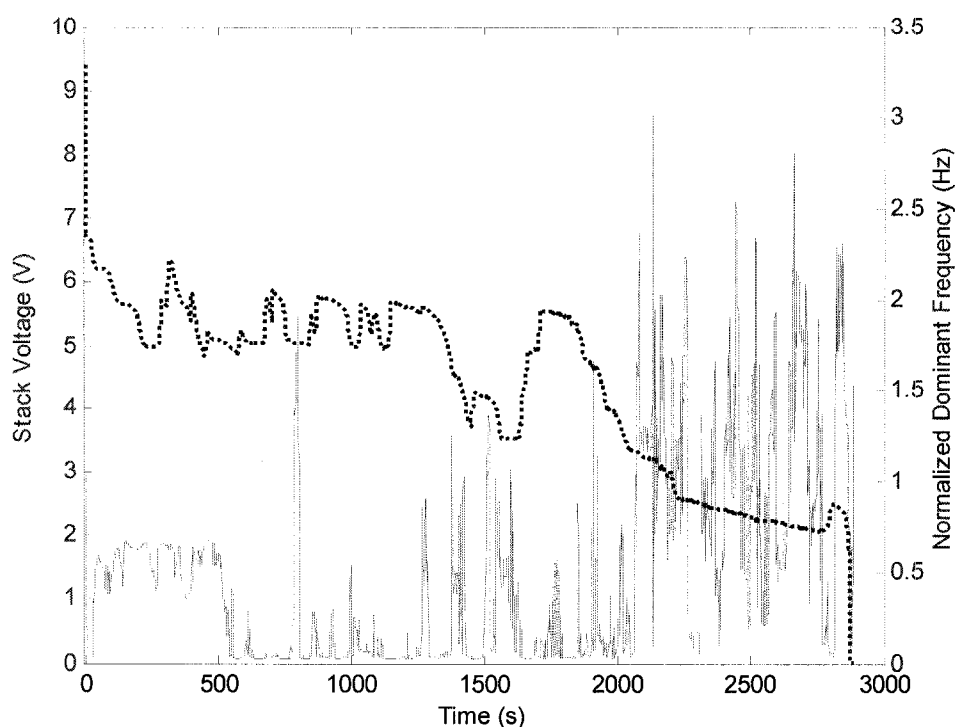


Fig. 31. Changes of dominant frequency of hydrogen/anode pressure drop and stack voltage with time when stack started from idle to 6 A load

Figs 28-31 present the anode pressure drop frequency changes with time for different start-up cases. Much more oscillations were observed compared with cathode pressure drop. The frequency peaks, again, were due to the water disturbance in the channels or even gas diffusion layer. For hydrogen, such disturbance was more obvious since its momentum was much lower than air. As a result, as long as there was certain amount of water at anode due to back diffusion, even in gas diffusion layer only, the frequency saw the oscillation. When more water was present at anode (see the areas of final voltage drop in Figs 28, 29, 31), such oscillation became more intense. However, due to the sensitivity of hydrogen pressure drop to water and the fact that water at anode

was from cathode, it may not be a good practice to use frequency of anode pressure drop as a diagnosis tool for the stack voltage.

4.3 Current step-up cases

4.3.1 Stack voltage responses

4.3.1.1 Non-oscillating cases

As mentioned in Table 2, current step-up cases were performed under the identical excess coefficients. Only when λ was fixed at 2 for air and 1.2 for hydrogen the stack oscillation was observed. When λ for air was maintained at 1.5 and 3 (scarce and excess air), stack voltage reached the new steady state after a period of time instead of oscillation. That is why in start-up cases, excess coefficient for air was fixed at 2 and for hydrogen 1.2. Under other conditions, unstable voltage oscillation, which is the focus of study, was not observed based on experimental experiences. Therefore, for these cases only stack voltage responses are presented.

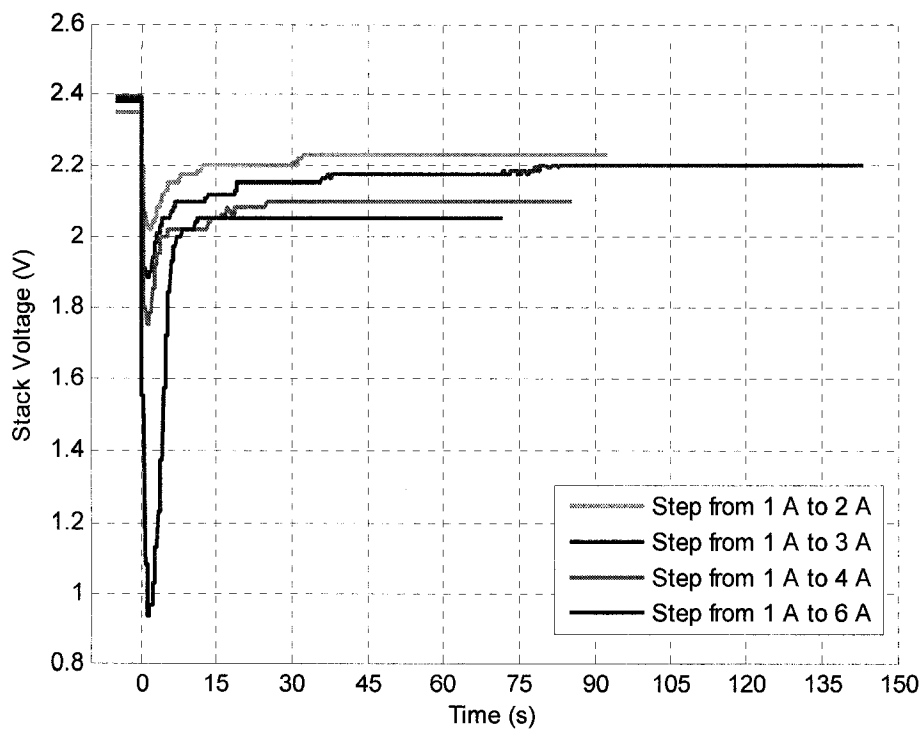


Fig. 32. Stack voltage responses after current step-up with excess coefficient fixed at 1.5 for air and 1.2 for hydrogen

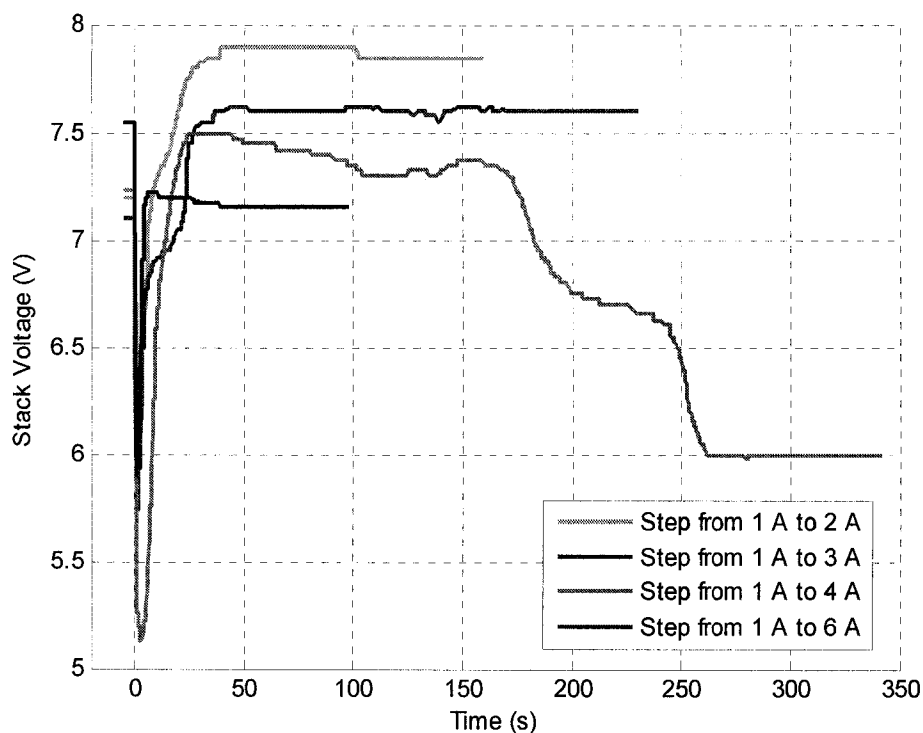


Fig. 33. Stack voltage responses after current step-up with excess coefficient fixed at 3 for air and 1.2 for hydrogen

Figs 32 and 33 show the stack voltage responses in such non-oscillating cases (case 1 and case 3 in Table 6). As shown in Fig 48, when excess coefficient for air was 1.5, before current step the stack voltage stabilized at about 2.4 V, indicating that only three cells were not flooded. It appears that air flow at excess coefficient of 1.5 was unable to remove the flooding water at any current load, steady state was therefore maintained. After current step-up, it took several minutes to stabilize, still only three cells being active. When excess coefficient for air was 3, which means the air flow was strong enough to remove flooding water; the steady state was also achievable. As shown in Fig 49, before current step at least nine cells were active with a total voltage of 7-7.6 V, after step-up the stack voltage either increased (1-2 A and 1-3 A cases) due to recovery of one

cell, or decrease due to inactivity of one flooding cell (1-4 A case) or the elevated current (1-6 A case). The flooding was still observed at one cell, and it cannot recover later. That is why oscillation was not observed when the air excess coefficient was high. It can be attributed to the fact that air flow removed water in other nine active cells maintained the reaction smoothly and evenly, except that there was serious fluctuation, the air flow could never pass the flooding cell due to its higher resistance. Such fluctuation seemingly did not happen at high air flow rate.

4.3.1.2 Oscillating cases

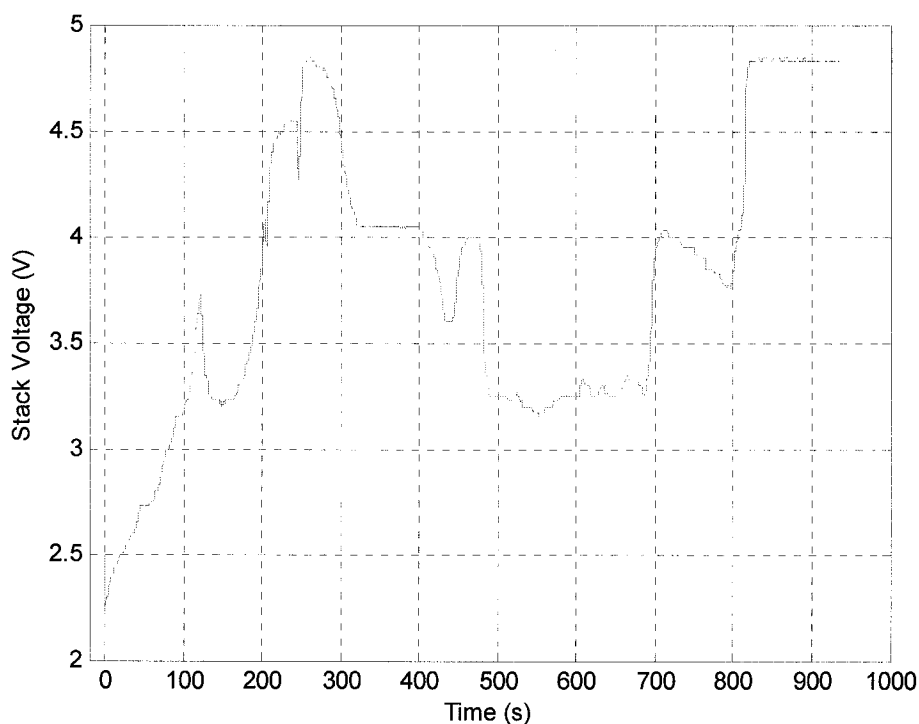


Fig. 34. Stack voltage response after current step-up from 1 A to 2 A with excess coefficient fixed at 2 for air and 1.2 for hydrogen

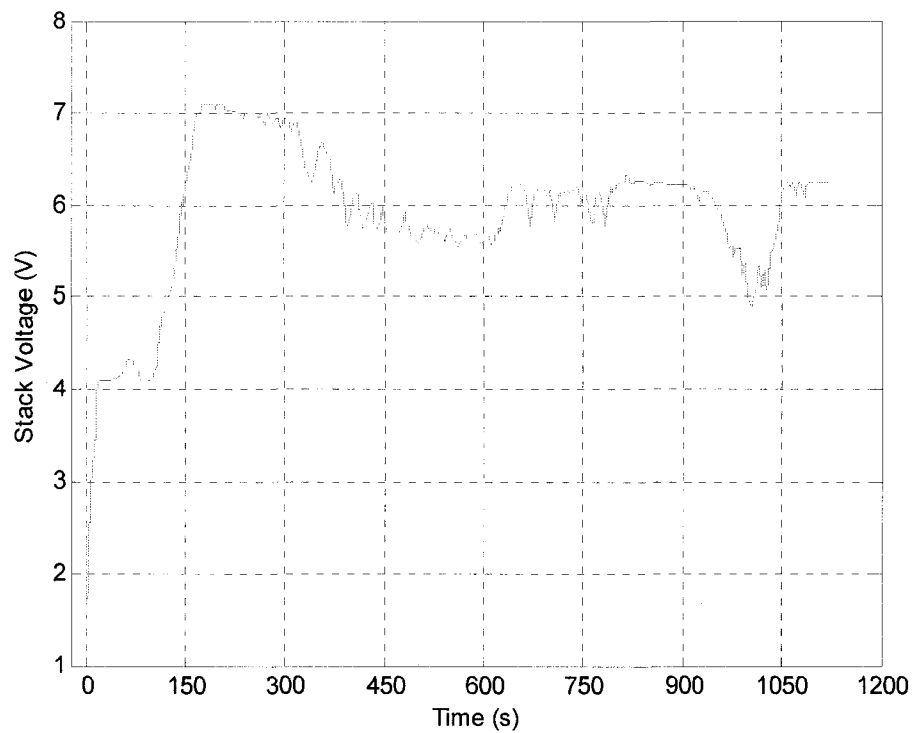


Fig. 35. Stack voltage response after current step-up from 1 A to 3 A with excess coefficient fixed at 2 for air and 1.2 for hydrogen

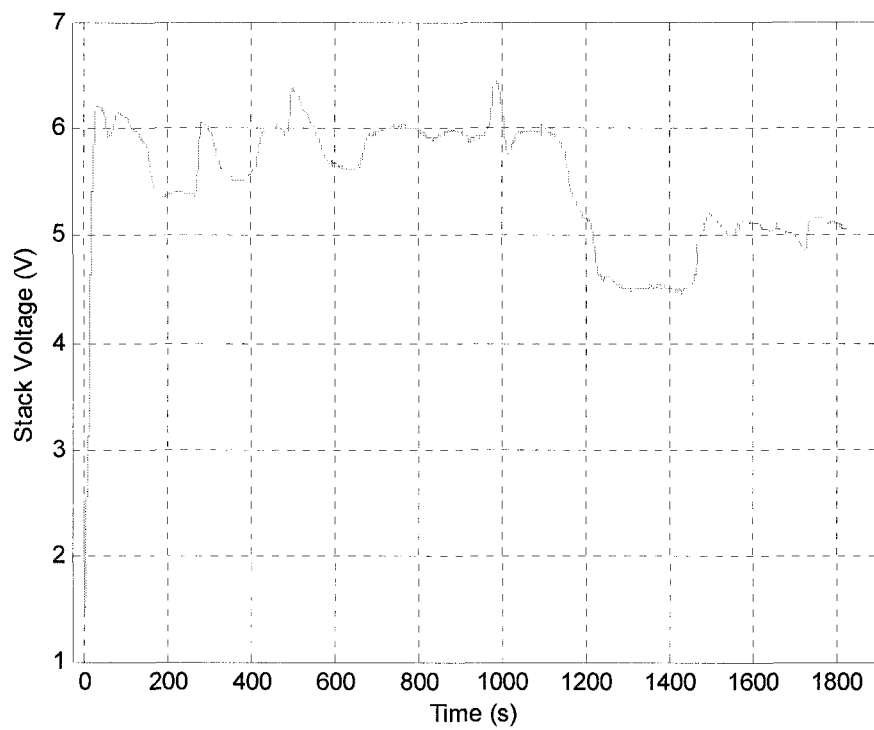


Fig. 36. Stack voltage response after current step-up from 1 A to 4 A with excess coefficient fixed at 2 for air and 1.2 for hydrogen

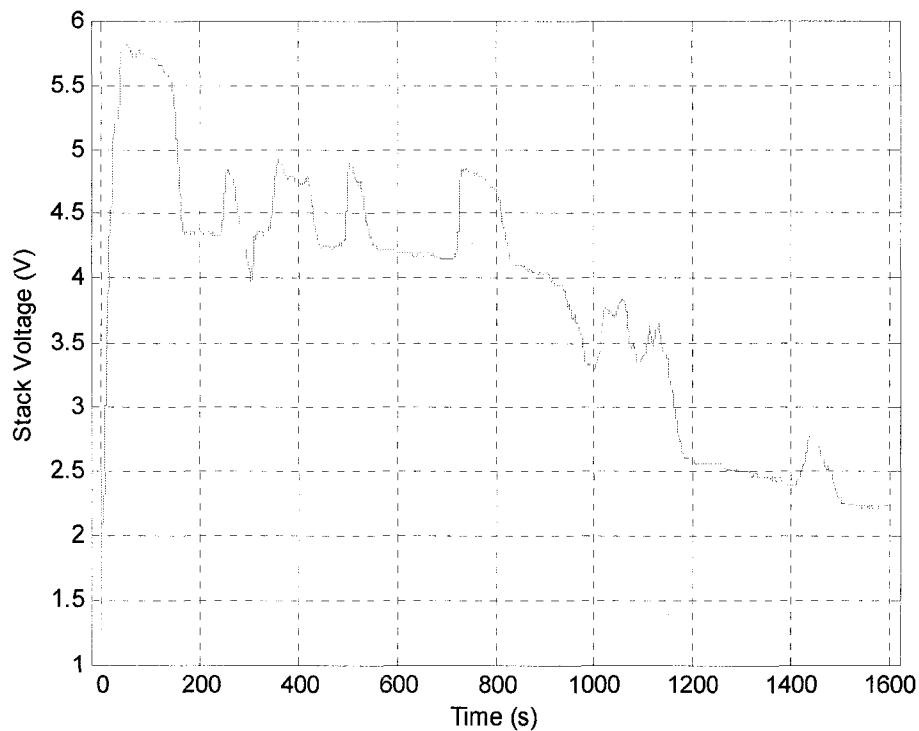


Fig. 37. Stack voltage response after current step-up from 1 A to 6 A with excess coefficient fixed at 2 for air and 1.2 for hydrogen

As shown in Figs 34-37, when air excess coefficient was fixed at 2, oscillation happened similar to the observations in start-up cases, which can be as well considered as responses under current step-up starting from zero. It can be concluded that air excess coefficient or flow rate determined the stack voltage oscillation, which must be at a medium level to oscillate the stack voltage. Excess coefficient of 2 is standard value for air in fuel cell industry; however, from the observations it is suggested a larger value may be preferred for stack operation, although the oscillation may also be attributed to the design and manufacturing problems specifically for the stack.

4.3.2 Pressure drop responses in time domain

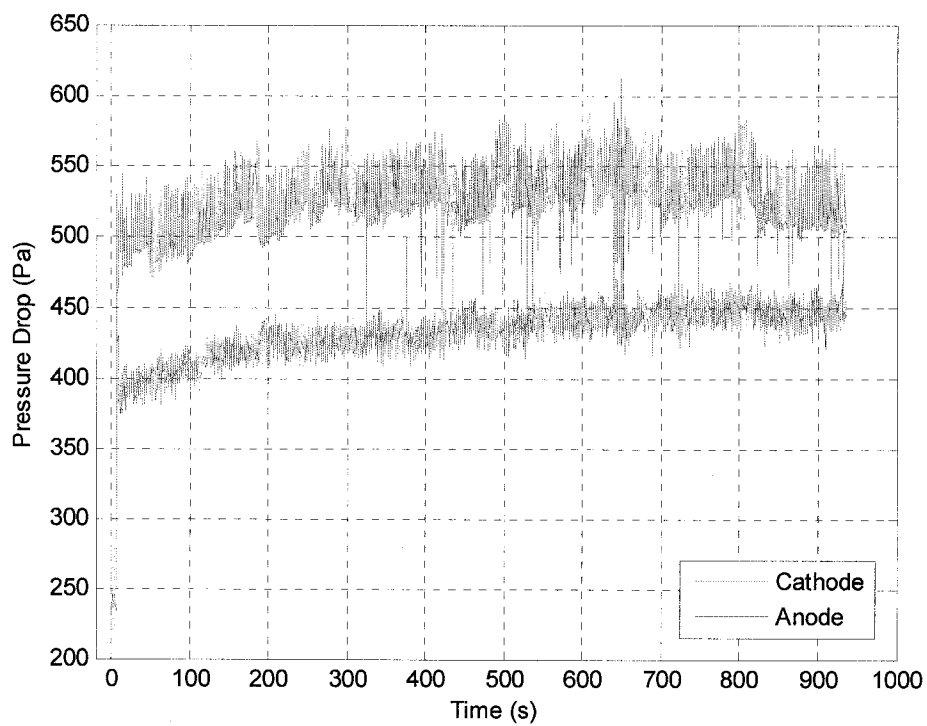


Fig. 38. Pressure drop response after current step-up from 1 A to 2 A

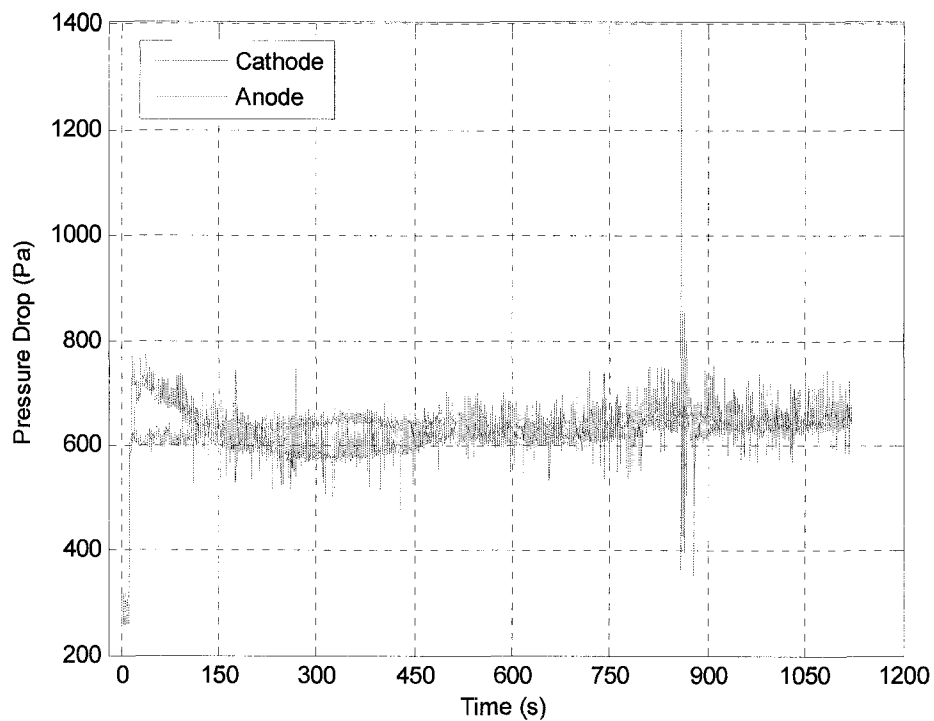


Fig. 39. Pressure drop response after current step-up from 1 A to 3 A

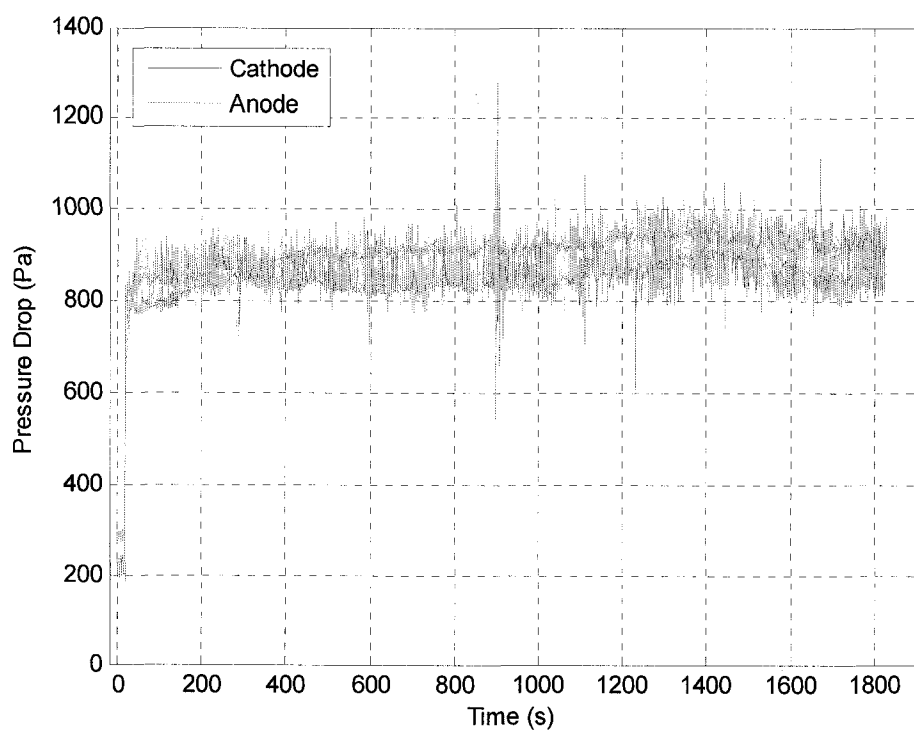


Fig. 40. Pressure drop response after current step-up from 1 A to 4 A

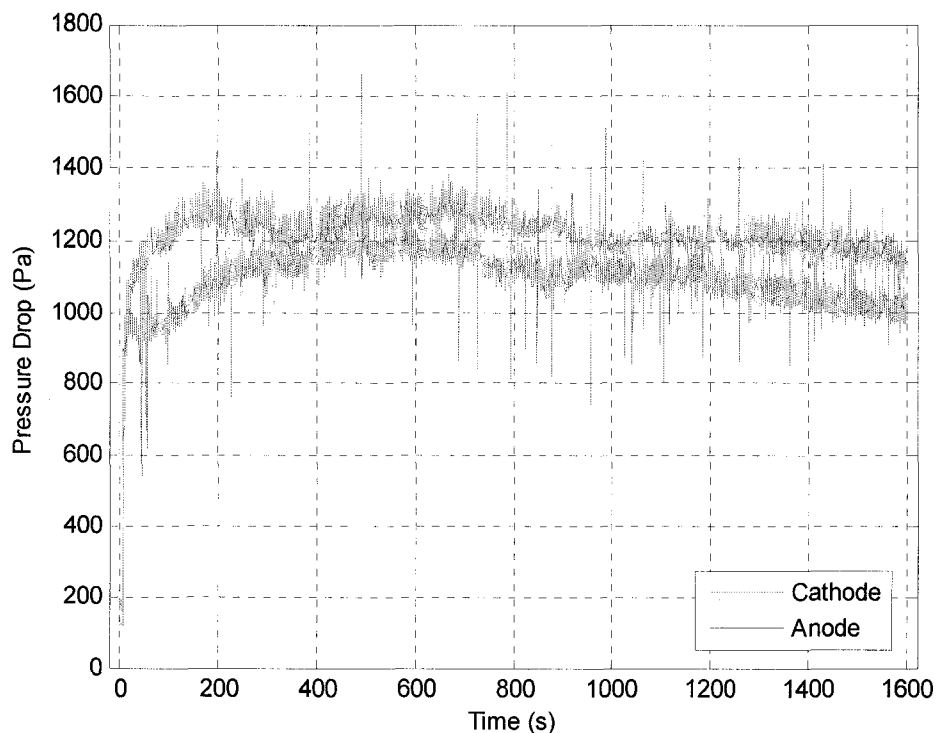


Fig. 41. Pressure drop response after current step-up from 1 A to 6 A

Only for those oscillation cases (excess coefficient fixed at 2 for air and 1.2 for hydrogen), pressure drop responses were recorded, as shown in Figs 38-41. Again, in time domain such signals contain high frequency oscillation that makes analysis difficult. The same data processing technique and procedures as in the start-up cases were applied. It is expected to correlate the dominant frequency of pressure drop signal with the stack voltage, as have been done in analysis of start-up cases.

4.3.3 Dominant frequencies of pressure drop signals

4.3.3.1 Dominant frequency of cathode pressure drop versus stack voltage

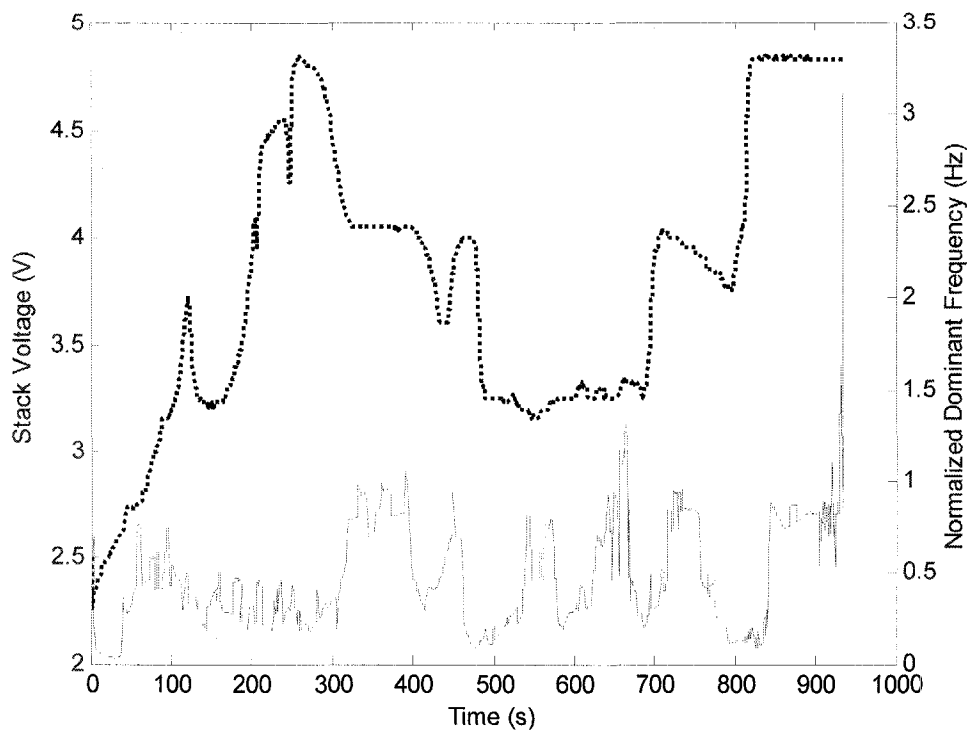


Fig. 42. Changes of dominant frequency of air/cathode pressure drop and stack voltage with time after current drawn from stack stepped up from 1 A to 2 A

As can be seen in Fig 42, the prediction rule that one or several intense frequency peaks during a period of stable stack voltage indicate there will be new “dead” cell generated still applies (see the peaks between 300 and 400 seconds). It can be also found in this case that before the stack voltage experienced an abrupt increase, i.e., recovery of one or two “dead” cells (see the voltage increase around 700 and 800 seconds), two signs were observed: 1) intense frequency peaks similar to previous rule; 2) unstable stack voltage but the change was small. Obviously, when air flow began to remove the flooding water, both cell voltage of that flooding cell and frequency of pressure drop was unstable. Note the small undershoot before the stack voltage increase around 800 seconds, as well

as the one before 200 seconds. Such undershoot can be explained in this way: the newly recovered cell began to generate water that partially blocked the gas diffusion layer again thereby increasing the mass transport loss; however such water was not dominant and was removed later by the air flow.

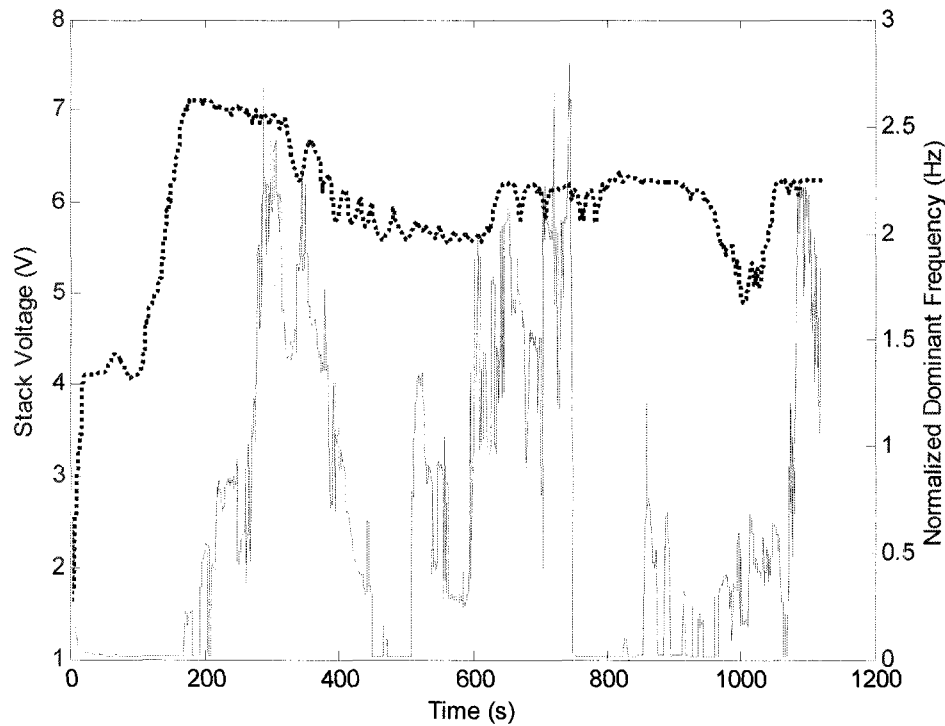


Fig. 43. Changes of dominant frequency of air/cathode pressure drop and stack voltage with time after current drawn from stack stepped up from 1 A to 3 A

As can be seen in Fig 43, after step-up to 3 A, the oscillation was not so obvious. From 200 to 800 seconds, it appeared that the flooding always stopped half way. In other words, water began to block the gas diffusion layer but was removed soon since the generation rate was insufficient under the air flow. The water activity in electrode caused the continuous frequency peaks between 200 and 800 seconds as well.

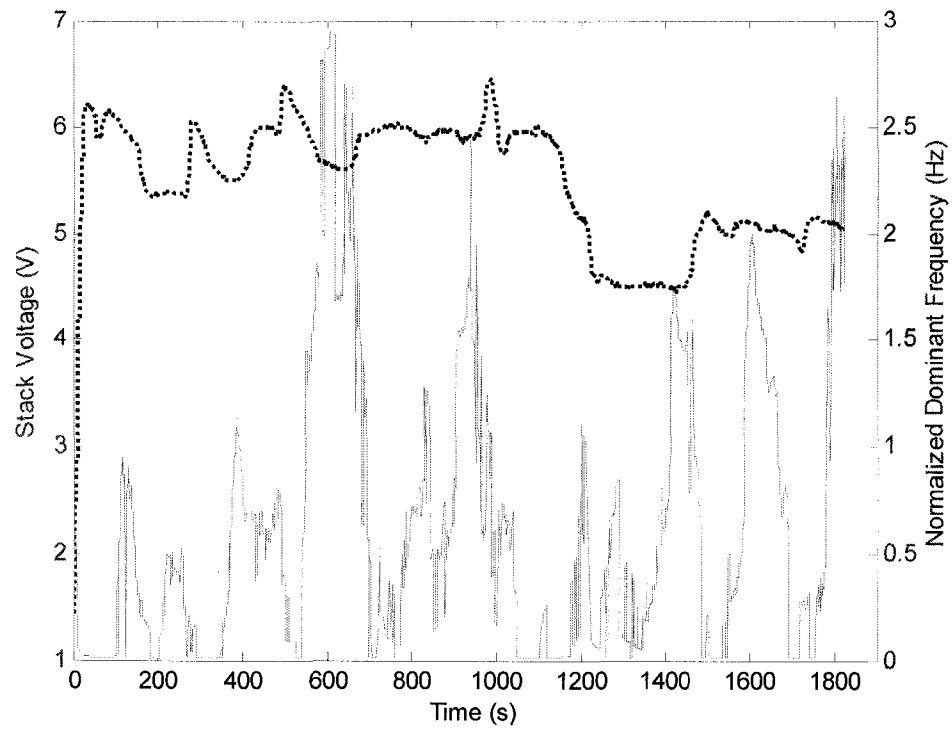


Fig. 44. Changes of dominant frequency of air/cathode pressure drop and stack voltage with time after current drawn from stack stepped up from 1 A to 4 A

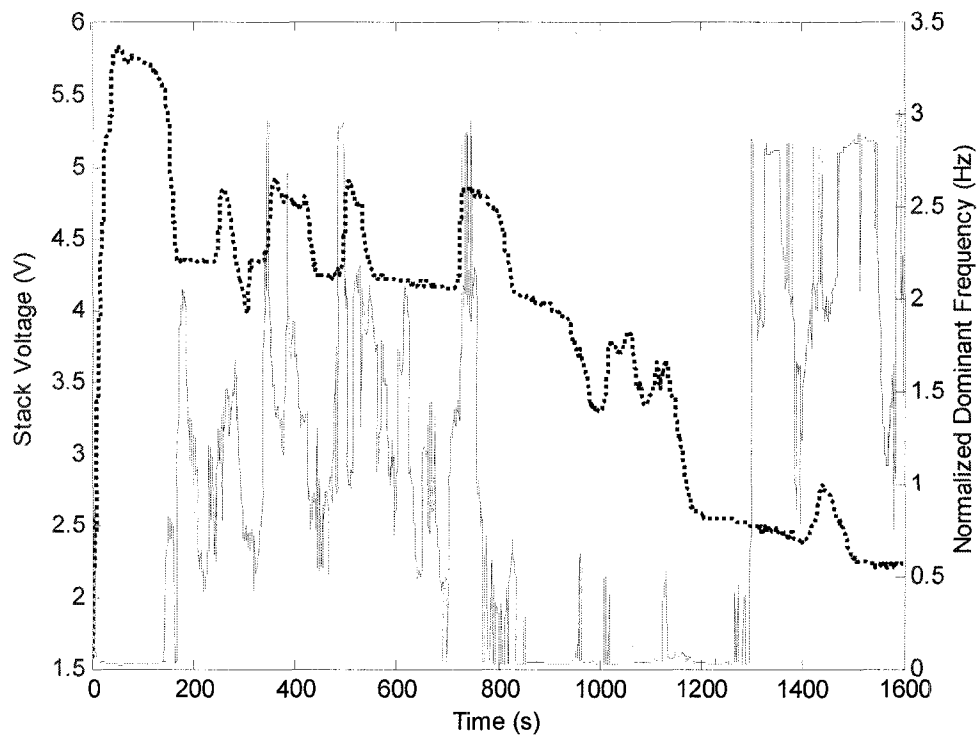


Fig. 45. Changes of dominant frequency of air/cathode pressure drop and stack voltage with time after current drawn from stack stepped up from 1 A to 6 A

In Figs 44 and 45, phase reverse between stack voltage and frequency signals was observed again (revisit Fig 41). The physics have been explained before. However, the stack voltage was far from an ideal periodic signal, therefore such phase reverse was not so accurate and not be always observed.

4.3.3.2 Dominant frequency of anode pressure drop versus stack voltage

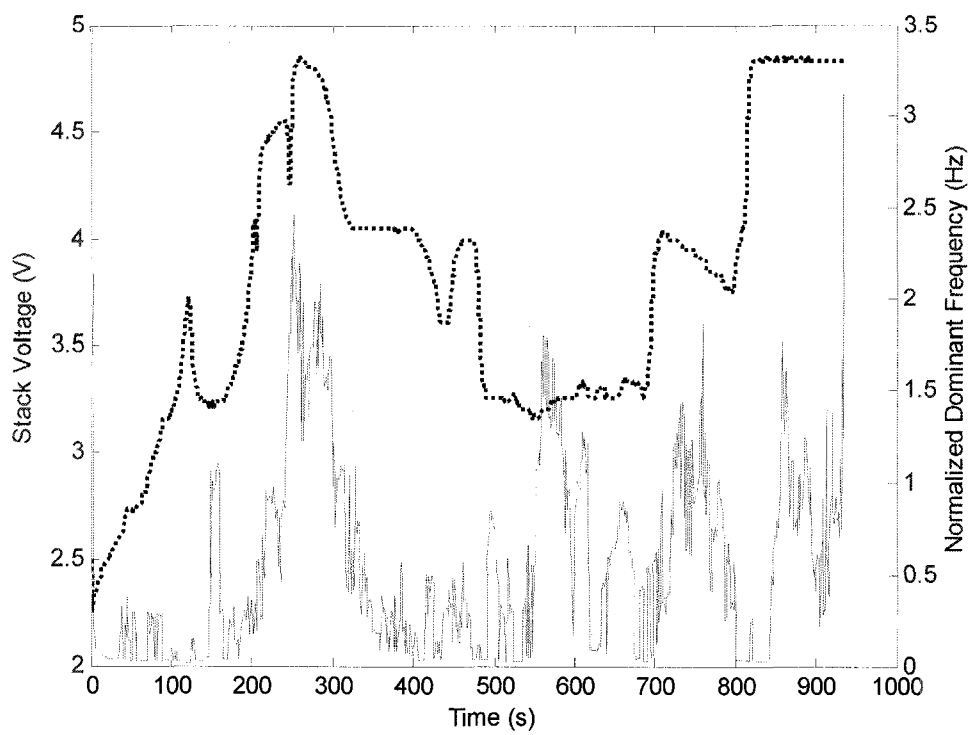


Fig. 46. Changes of dominant frequency of hydrogen/anode pressure drop and stack voltage with time after current drawn from stack stepped up from 1 A to 2 A

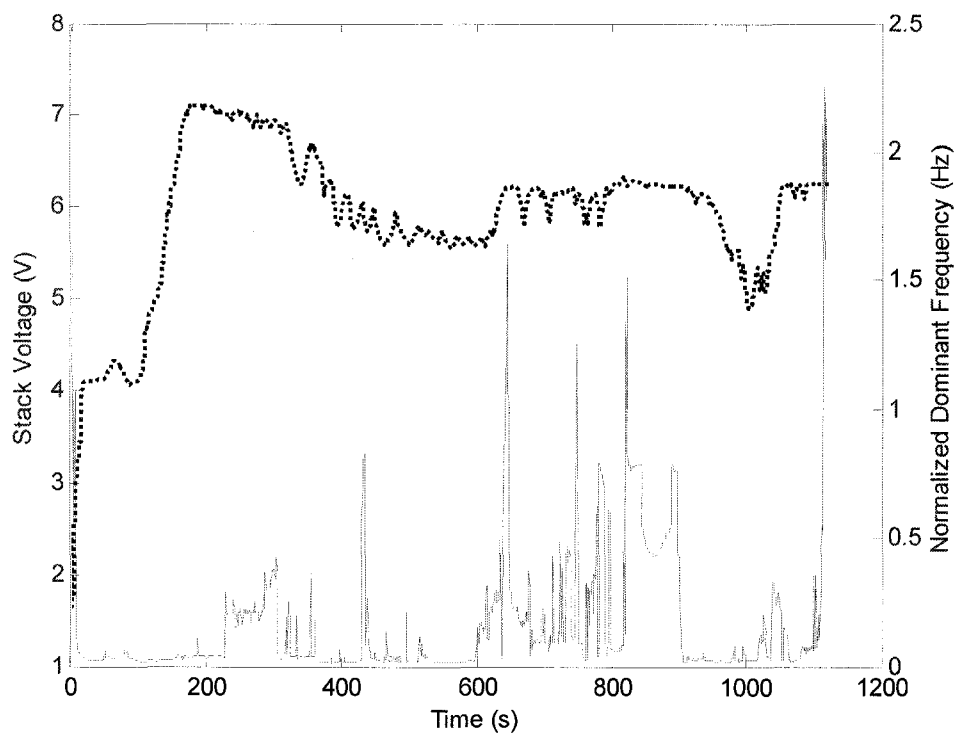


Fig. 47. Changes of dominant frequency of hydrogen/anode pressure drop and stack voltage with time after current drawn from stack stepped up from 1 A to 3 A

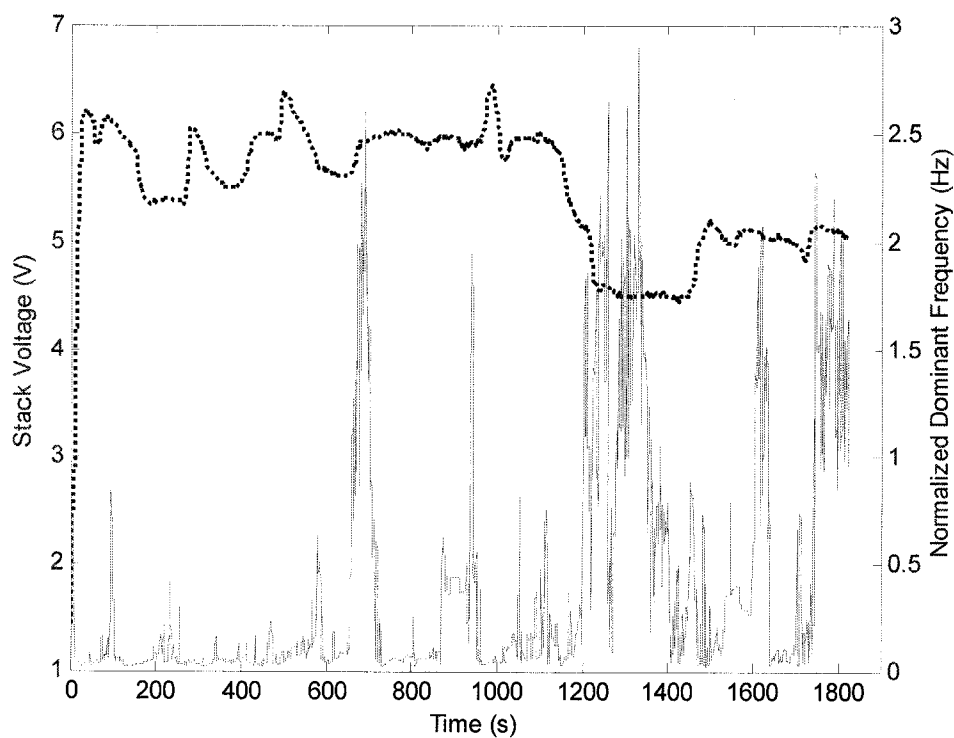


Fig. 48. Changes of dominant frequency of hydrogen/anode pressure drop and stack voltage with time after current drawn from stack stepped up from 1 A to 4 A

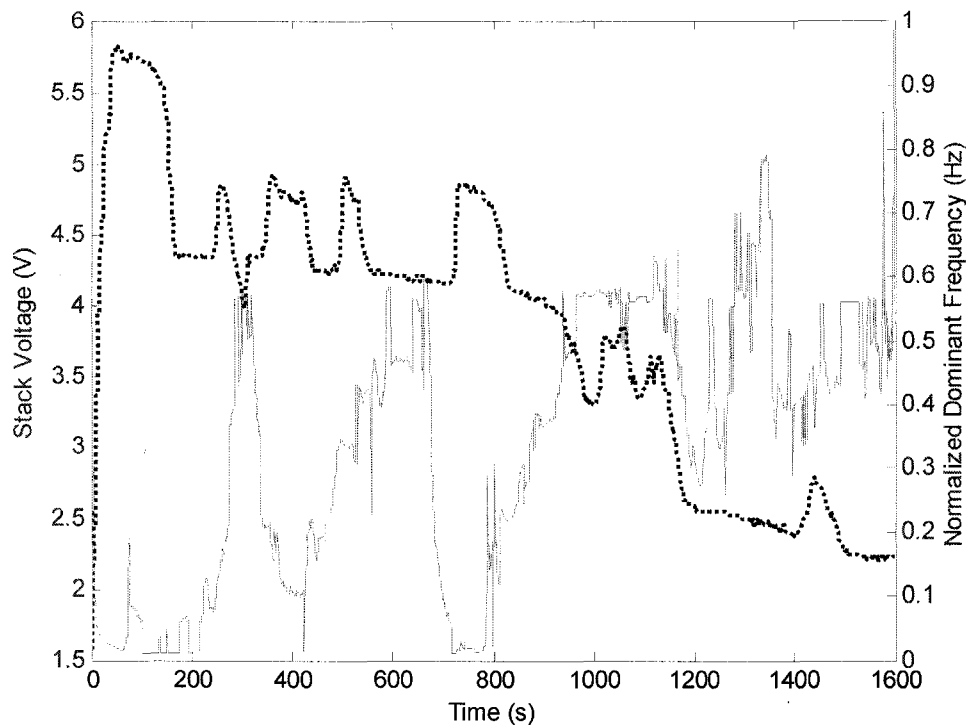


Fig. 49. Changes of dominant frequency of hydrogen/anode pressure drop and stack voltage with time after current drawn from stack stepped up from 1 A to 6 A

For frequency of anode pressure drop, as analyzed in start-up cases, it is a direct indication of water amount at anode. Figs 62, 64, 65 present a common characteristic that before an abrupt stack voltage increase, there were usually frequency peaks observed, which suggested increasing amount of water at that time. It can be therefore inferred that the flooding water at cathode was diffusing back to anode, thereby contributing to the recovery of “dead” cell. The sufficient air flow probably not only blows away flooding water but also facilitates the water back-diffusion through the membrane to anode.

CHAPTER V

CONCLUSIONS AND RECOMMENDATIONS

5.1 Conclusions

In this study, the steady state performance and dynamic behavior of a commercial 10-cell fuel cell stack was investigated using a self-developed PEM fuel cell testing stand. Experimental data in terms of stack voltage, temperature and pressure drop were presented and analyzed. It was found when air excess coefficient was fixed at 2, the stack voltage experienced obvious and long-time oscillation after either the stack started from idle to a constant current load or stepped up from 1 A to an elevated current. In order to correlate stack voltage with cathode/anode pressure drop, fast Fourier transform (FFT) technique and specifically designed data processing procedure was applied to find the dominant frequency of pressure drop, which successfully revealed the relationship between. Dominant frequency of cathode pressure drop was observed to predict the abrupt stack voltage increase and decrease. Peak of dominant frequency of cathode pressure drop was found to be an indication that cathode water flooding starts. Phase reverse between dominant frequency and stack voltage was also observed in start-up to 2 A and 4 A load cases. These relationships exist because changes of dominant frequency and stack voltage are due to the same physics, that is, the water flooding-removal cycle in cathode. For dominant frequency of anode pressure drop, it was a direct indication of water amount at anode, peak of which can be considered a sign of sudden presence of water at anode. Such water was usually from the cathode due to the back-diffusion.

5.2 Recommendations

It is potentially possible for the pressure drop signal to be utilized as a diagnosis tool for stack voltage. Furthermore, in a PEM fuel cell power system, the stack output can be predicted by pressure drop signal and then controlled by adjusting flow rate of reactants. However, for this purpose, more experiments are necessary to collect data for different configurations of fuel cell stack under different operating conditions so that a mathematical model describing such relationship can be developed, which could be most challenging. Additionally, algorithm to determine the optimum window size in performing FFT may also be necessary to guarantee that the dominant frequency information is well retained whereas less noise is present.

REFERENCES

- [1] J. Larminie and A. Dicks, in Fuel Cell System Explained, John Wiley & Sons, 2003, P. 22-29.
- [2] J. Larminie and A. Dicks, in Fuel Cell System Explained, John Wiley & Sons, 2003, P. 45-66.
- [3] R. O'Hayre, S. Cha, W. Colella and F. Prinz, in Fuel Cell Fundamentals, John Wiley & Sons, 2006, P. 206-207.
- [4] D. Liu and S. Case, Journal of Power Sources, 162, (2006) 521-531.
- [5] W. Hogarth and J. Benziger, Journal of Power Sources, 159, (2006) 968-978.
- [6] J. Park and X. Li, Journal of Power Sources, 163, (2007) 853-863.
- [7] <http://www.fideris.com/>
- [8] <http://www.fuelcell.com/>
- [9] S. Dutta, S. Shimpalee and J. Zee, Journal of Applied Electrochemistry, 30, (2000) 135-146.
- [10] J. Amphlett, R. Mann, B. Peppley, P. Roberge and A. Rodrigues, Journal of Power Sources, 61, (1996) 183-188.
- [11] M. Ceraolo, C. Miulli and A. Pozio, Journal of Power Sources, 113, (2003) 131-144.
- [12] T. Berning and N. Djilali, Journal of Electrochemical Society, 150, (2003) A1589-1598.
- [13] X. Xue, J. Tang, A. Smirnova, R. England and N. Sammes, Journal of Power Sources, 133, (2004) 188-204.
- [14] S. Shimpalee, W. Lee, J. Zee and H. Naseri-Neshat, Journal of Power Sources, 156, (2006) 355-368.

- [15] S. Shimpalee, W. Lee, J. Zee and H. Naseri-Neshat, *Journal of Power Sources*, 156, (2006) 369-374.
- [16] X. Yu, B. Zhou and A. Sobiesiak, *Journal of Power Sources*, 147, (2005) 184-195.
- [17] Y. Wang and C.-Y. Wang, *Electrochimica Acta*, 50, (2005) 1307-1315.
- [18] Y. Wang and C.-Y. Wang, *Electrochimica Acta*, 51, (2006) 3924-3933.
- [19] J. Hamelin, K. Agbossou, A. Laperriere, F. Laurenfuel celle and T. Bose, *International Journal of Hydrogen Energy*, 26, (2001) 625-629.
- [20] S. Morner and S. Klein, *Journal of Solar Energy Engineering*, 123, (2001) 225-231.
- [21] S. Kim, S. Shimpalee and J. Zee, *Journal of Power Sources*, 137, (2004) 43-52.
- [22] S. Kim, S. Shimpalee and J. Zee, *Journal of Power Sources*, 135, (2004) 110-121.
- [23] Q. Yan, H. Toghiani and H. Causey, *Journal of Power Sources*, 161, (2006) 492-502.
- [24] F. Philipps, G. Simons and K. Schiefer, *Journal of Power Sources*, 154, (2006) 412-419.
- [25] F. Barbir, H. Gorgun and X. Wang, *Journal of Power Sources*, 141, (2005), 96-101.
- [26] W. He, G. Lin and T. V. Nguyen, *AIChE Journal*, 49 (12), (2003), 3221-3228.
- [27] Y. Zong, B. Zhou and A. Sobiesiak, *Journal of Power Sources*, 161, (2006), 143-159.
- [28] <http://www.fuelcells.org.au/Fuel-Cell-Education-NSW-Australia.htm>
- [29] Palcan Fuel Cells Ltd., PC3 Air-cool Fuel Cell Stack User's Manual, 2006.

VITA AUCTORIS

Jixin Chen, born on March 29, 1983 in the city of Hangzhou, Zhejiang Province, China, received his high school diploma from Hangzhou No.2 High School in 2001. From 2001-2005 he was an undergraduate student at Hefei University of Technology majoring Testing and Control Technique and Instrument, where he received the degree of Bachelor of Applied Science in June 2005. He went to University of Windsor for his Master study in Mechanical Engineering and will receive the degree of Master of Applied Science in October 2007. He will attend University of California, Irvine for his Ph.D. study in Mechanical Engineering.